Cellular/Molecular

Mitochondrial Ca^{2+} Cycling Facilitates Activation of the Transcription Factor NFAT in Sensory Neurons

Man-Su Kim and Yuriy M. Usachev
Department of Pharmacology, University of Iowa Carver College of Medicine, Iowa City, Iowa 52242

Ca^{2+}-dependent gene regulation controls many aspects of neuronal plasticity. Significant progress has been made toward understanding the roles of voltage- and ligand-gated Ca^{2+} channels in triggering specific transcriptional responses. In contrast, the functional importance of Ca^{2+} buffers and Ca^{2+} transporters in neuronal gene regulation is less clear despite their critical contribution to the spatiotemporal control of Ca^{2+} signals. Here we examined the role of mitochondrial Ca^{2+} uptake and release in regulating the Ca^{2+}-dependent transcription factor NFAT (nuclear factor of activated T-cells), which has been implicated in synaptic plasticity, axonal growth, and neuronal survival. Intense stimulation of sensory neurons by action potentials or TRPV1 agonists induced rapid activation and nuclear import of NFAT. Nuclear translocation of NFAT was associated with a characteristic prolonged $[Ca^{2+}]_i$ elevation (plateau) that resulted from Ca^{2+} uptake by, and its subsequent release from, mitochondria. Measurements using a mitochondrial Ca^{2+} indicator, mtPericam, showed that this process recruited mitochondria throughout the cell body, including the perinuclear region. $[Ca^{2+}]_i$ levels attained during the plateau phase were similar to or higher than those required for NFAT activation (200–300 nM). The elimination of the $[Ca^{2+}]_i$ plateau by blocking either mitochondrial Ca^{2+} uptake via the uniporter or Ca^{2+} release via the mitochondrial Na^+/Ca^{2+} exchanger strongly reduced nuclear import of NFAT. Furthermore, preventing Ca^{2+} mobilization via the mitochondrial Na^+/Ca^{2+} exchanger diminished NFAT-mediated transcription. Collectively, these data implicate activity-induced Ca^{2+} uptake and prolonged release from mitochondria as a novel regulatory mechanism in neuronal excitation–transcription coupling.

Introduction

Activity-dependent gene regulation underlies many forms of neuronal plasticity, including structural and functional changes that take place during development, synaptic remodeling associated with learning and memory formation, and long-term alteration of neuronal function in neurological disorders (Deisseroth et al., 2003; Cohen and Greenberg, 2008). Ca^{2+} plays the central role in these processes by coupling electrical activity to the activation of various Ca^{2+}-dependent transcription factors. One of the fundamental questions of Ca^{2+}-dependent gene regulation is how the spatiotemporal organization of neuronal Ca^{2+} signals determines the transcriptional outcome. Recent studies established the importance of the Ca^{2+} entry mechanisms (e.g., via NMDA receptors versus the L-type Ca^{2+} channels) in triggering specific transcription pathways (Deisseroth et al., 2003; Greer and Greenberg, 2008). In contrast, the role of Ca^{2+} pumps, exchangers, and Ca^{2+}-transporting organelles in neuronal gene regulation is poorly understood, despite the fact that these systems profoundly affect the amplitude, duration, and subcellular localization of Ca^{2+} signals produced by neuronal activity (Miller, 1991; Thayer et al., 2002). In this study we examined how Ca^{2+} uptake and release by mitochondria contributes to neuronal regulation of the transcription factor NFAT (nuclear factor of activated T-cells).

NFAT is a Ca^{2+}/calcineurin (CaN)-dependent transcription factor that has been implicated in the development and function of various organ systems, including the immune, endocrine, and cardiovascular systems (Crabtree and Olson, 2002; Hogan et al., 2003). Recent studies have highlighted the importance of NFAT in neurons, where it is activated by electrical activity and neurotrophins and is involved in the control of synaptic plasticity, axonal growth, and neuronal survival (Graef et al., 1999, 2003; Groth and Mermelstein, 2003; Benedito et al., 2005; Oliveria et al., 2007). NFAT is exquisitely sensitive to the duration of the Ca^{2+} signal (Dolmetsch et al., 1997), which is explained by its activation mechanisms. In resting cells, phosphorylated NFAT resides in the cytosol. It is dephosphorylated by CaN in response to an increase in $[Ca^{2+}]_i$, resulting in unmasking of its nuclear localization signal (NLS) and its import into the nucleus. There, NFAT partners with other transcription factors to initiate transcription. Once $[Ca^{2+}]_i$ returns to basal levels, glycogen synthase kinase-3β (GSK3β) and several other protein kinases rephosphorylate NFAT, which promotes Crm-1-mediated NFAT export from the nucleus (Crabtree and Olson, 2002; Hogan et al., 2003). Thus, NFAT-mediated transcriptional responses depend on the balance between the activities of CaN and NFAT kinases. Consequently, retaining NFAT in the

Received July 14, 2009; accepted Aug. 14, 2009.

This work was supported by National Institutes of Health Grant NS054614 and an American Heart Association National Scientist Development Grant to Y.M.U. M.-S.K. is a predoctoral fellow of the American Heart Association, Midwest Affiliate. We thank Drs. Stanley Thayer and Paul Mermelstein for their support and help in the initiation of this work, Drs. Johannes Hell and Stefan Strack for helpful comments on this manuscript, Dr. Anjana Rao for the EGFP-NFAT1 (c2) plasmid, Dr. Eric Olson for the EGFP-NFAT2 (c1) plasmid, Dr. Masamitsu Iino for the GFP-NFAT4 (c3) plasmid, Dr. Isabella Graef for the EGFP-NFATc4 plasmid, and Dr. Atsushi Miyawaki for the mtPericam plasmid.

Correspondence should be addressed to Yuriy M. Usachev, Department of Pharmacology, University of Iowa Carver College of Medicine, 2-250 BSB, 51 Newton Road, Iowa City, IA 52242. E-mail: yuriy-usachev@uiowa.edu.

DOI:10.1523/JNEUROSCI.3384-09.2009

 0270-6474/09/2912101-14$15.00/0

nucleus requires continuous CaN activity and persistent $[Ca^{2+}]_i$ elevation.

In lymphocytes and other nonexcitable cells, the prolonged $[Ca^{2+}]_i$ elevation essential for NFAT signaling is mediated by so-called Ca^{2+} release-activated Ca^{2+} channels or CRACs (Feske et al., 2006). In neurons, however, the nature of the mechanisms that sustain NFAT activation is not fully understood. Here, by simultaneously imaging $[Ca^{2+}]_i$ changes and NFAT dynamics within single neurons, and by monitoring expression of NFAT-reporter genes, we demonstrate for the first time that prolonged Ca^{2+} release from mitochondria significantly contributes to NFAT activation in neurons and facilitates the function of NFAT as a nuclear integrator of repetitive electrical activity.

Materials and Methods

Cell cultures and transfection. Cultures of DRG neurons were prepared from newborn Sprague Dawley rats, as previously described (Usachev and Thayer, 1999). In brief, newborn (1- to 3-d-old) Sprague Dawley rats (Charles River Laboratories) were killed according to a protocol approved by the University of Iowa Institutional Animal Care and Use Committee. DRGs were dissected from the thoracic and lumbar segments and incubated in Pronase E dissolved in DMEM (1 mg/ml) for 7 min at 37°C in a 10% CO_2 incubator. Ganglia were washed twice in cold DMEM containing HEPES (20 mM; pH, 7.4) and then mechanically dissociated by trituration with flame-constricted Pasteur pipettes of decreasing diameter. Suspensions of DRG cells were plated onto 25 mm glass coverslips coated with poly-L-ornithine and laminin. Cells were grown in DMEM supplemented with 5% heat-inactivated horse serum, 5% fetal bovine serum, and penicillin–streptomycin (100 U/ml and 100 μg/ml, respectively) in a 10% CO_2 incubator at 37°C and used within 2–3 d after plating. Transfection of DRG neurons was performed before plating, using an Amaxa electroporation system (Program G-13), as previously described (Schnizler et al., 2008), except for the experiments shown in Figure 1*D*, for which the cells were transfected using gene gun (Usachev et al., 2002). The EGFP-NFAT1 (c2) plasmid was a gift from Dr. A. Rao (Harvard University, Cambridge, MA) (Aramburu et al., 1999), the EGFP-NFAT2 (c1) plasmid was a gift from Dr. E. Olson (University of Texas Southwestern Medical Center, Dallas, TX) (Chin et al., 1998), the GFP-NFAT4 (c3) plasmid was a gift from Dr. M. Iino (The Tokyo Metropolitan Institute of Medical Science, Tokyo, Japan) (Tomida et al., 2003), the EGFP-NFATc4 plasmid was a gift from Dr. I. Graef (Stanford University, Stanford, CA) (Graef et al., 1999) and was also obtained from Addgene (plasmid 10961), and the mtPericam plasmid was a gift from Dr. A. Miyawaki (RIKEN, Tokyo, Japan) (Nagai et al., 2001).

Simultaneous imaging of $[Ca^{2+}]_i$ and (E)GFP-labeled NFAT isoforms. DRG neurons were transfected with one of the following plasmids: EGFP-NFATc1, EGFP-NFATc2, GFP-NFATc3, or EGFP-NFATc4. Then, in 24–48 h, cells were loaded with the Ca^{2+}-sensitive indicator fura-2 (fura-2 AM). Cells were placed in a flow-through chamber mounted on the stage of an inverted IX-71 microscope (Olympus) and perfused with the standard extracellular HEPES-buffered Hank's salt solution (HH buffer) composed of the following (in mM): 140 NaCl, 5 KCl, 1.3 $CaCl_2$, 0.4 $MgSO_4$, 0.5 $MgCl_2$, 0.4 KH_2PO_4, 0.6 $NaHPO_4$, 3 $NaHCO_3$, 10 glucose, 10 HEPES, pH 7.4, with NaOH (310 mOsm/kg with sucrose). Fluorescence was alternately excited at 340 (12 nm bandpass), 380 (12) nm, and 475 (12) nm using the Polychrome IV monochromator (TILL Photonics) and focused on the cells via a 40× oil-immersion objective (NA = 1.35, Olympus). Emitted fluorescence was collected at 530 (50) nm using an IMAGO CCD camera (640 × 480 pixels; TILL Photonics). A 2 × 2 binning of the camera (each pixel corresponds to ~500 nm) was used for most of the experiments, except for those shown in supplemental Figures 3*C*,*D* and 4*A*–*C*, available at www.jneurosci.org as supplemental material, for which the CCD camera was used at its maximal spatial resolution (no binning; each pixel corresponds to ~250 nm). Series of 340, 380, and 475 nm images were sampled every 5, 10, or 20 s. Fluorescence was corrected for background at each wavelength, as determined in an area that did not contain any cell. The fluorescence ratio ($r = F_{340}/F_{380}$) was converted to $[Ca^{2+}]_i$ according to the following formula: $[Ca^{2+}]_i = K_d\beta(R - R_{min})/(R_{max} - R)$ (Grynkiewicz et al., 1985). R_{min}, R_{max}, and β were determined by applying 10 μM ionomycin in Ca^{2+}-free buffer (1 mM EGTA) and HH buffer (1.3 mM Ca^{2+}) (Usachev and Thayer, 1999). Translocation of (E)GFP-labeled NFAT isoforms was analyzed by calculating mean intensities of (E)GFP fluorescence in the cytosol and nucleus and expressed as the (E)GFP-NFAT nuclear/cytosolic ratio. Data were processed using TILLvisION 4.0.1.2 (TILL Photonics) software and presented as mean ± SEM.

$[Ca^{2+}]_i$ elevation and nuclear import of NFAT isoforms were induced by trains of action potentials, TRPV1 agonists, or high-K^+-induced depolarization. Two different depolarization protocols were used throughout the study. For the first protocol, strong depolarization was evoked by a brief (30 or 180 s) application of 90 mM KCl (K^+90). Such stimulation produced large-amplitude $[Ca^{2+}]_i$ elevations (>1 μM), which engaged mitochondria and led to the generation of prolonged $[Ca^{2+}]_i$ plateau and robust NFAT translocation and essentially mimicked the $[Ca^{2+}]_i$ and NFAT responses induced by trains of action potentials or by TRPV1 agonists. The second depolarization protocol was designed to generate sustained $[Ca^{2+}]_i$ elevations of relatively small amplitude (<300–500 nM), which are independent of mitochondria. For this weak-depolarization protocol, 10, 15, 20, or 25 mM KCl was applied for various time periods ranging from 10 to 60 min, which, in turn, determined the duration of $[Ca^{2+}]_i$ elevations. Indeed, no $[Ca^{2+}]_i$ plateau was observed for such weak depolarizations, and $[Ca^{2+}]_i$ rapidly returned toward the baseline upon repolarization. In this protocol, the L-type Ca^{2+} channel activator BayK8644 (1 μM) was added to the K^+10, K^+15, K^+20, and K^+25 solutions, as we found that this drug helped to stabilize $[Ca^{2+}]_i$ at the corresponding elevated levels.

In some experiments $[Ca^{2+}]_i$ elevations and nuclear import of NFAT were induced by the Ca^{2+} ionophore ionomycin (10 μM). Extracellular Ca^{2+} concentration ($[Ca^{2+}]_o$) was set to the low submicromolar levels in these experiments by mixing 5 mM EGTA with either 4.3 or 4.4 mM $CaCl_2$ in the extracellular solution of the following composition (in mM): 140 NaCl, 5 KCl, 1 $MgCl_2$, 10 glucose, 10 HEPES, pH 7.4, with NaOH (310 mOsm/kg with sucrose). The resulting $[Ca^{2+}]_o$ was determined by fluorescent microscopy using a 100 μl droplet of the described solutions supplied with 50 μM fura-2. Combining 5 mM EGTA and 4.3 mM $CaCl_2$ yielded a $[Ca^{2+}]_o$ of 171 ± 8 nM ($n = 5$ independent measurements); a combination of 5 mM EGTA with 4.4 mM $CaCl_2$ yielded a $[Ca^{2+}]_o$ of 255 ± 24 nM ($n = 5$ independent measurements).

Measurement of mitochondrial Ca^{2+} concentration $[Ca^{2+}]_{mt}$. Mitochondrial Ca^{2+} concentration ($[Ca^{2+}]_{mt}$) was measured using the mitochondrion-targeted Ca^{2+} indicator mtPericam (Nagai et al., 2001), as previously described (Medvedeva et al., 2008). mtPericam fluorescence was excited at 410 (12) nm via a 60× oil-immersion objective (NA = 1.40, Olympus) and collected at 530 (50) nm at the sampling rate of 0.2 Hz (Fig. 2*F*) or 2 and 10 Hz (Fig. 2*E*) using the same fluorescent microscope as described above. A 2 × 2 digital binning was used in these experiments, which corresponds to ~330 nm/pixel (60× objective; 640 × 480 pixels IMAGO CCD camera; TILL Photonics). $[Ca^{2+}]_{mt}$ changes were presented as $-\Delta F/F_0 = -(F - F_0)/F_0$, where F is current fluorescence intensity and F_0 is fluorescence intensity in the resting cell. Fluorescence was corrected for background, as determined in an area that did not contain any cell.

Gene reporter assays. DRG neurons were transfected with the NFAT-luciferase (firefly) reporter plasmid (2.5 μg of cDNA/reaction; pNFAT-TA-luciferase; Clontech) alone or together with a plasmid encoding a *Renilla reniformis* luciferase controlled by a constitutive HSV-thymidine kinase (TK) promoter (0.25 μg of cDNA/reaction; pRL-TK; Promega). On the next day, cells were stimulated with K^+10, K^+15, K^+20, or K^+25 solutions (prepared by mixing 150 mM KCl with complete DMEM) containing 1 μM BayK8644 for various durations (see Results for details). Specifically, for the experiments described in Figure 1*C*, which examined NFAT activation as a function of the duration of depolarization (and $[Ca^{2+}]_i$ elevation), the periods of depolarization using K^+20 were 2, 6, and 12 h. For the experiments described in Figure 3, *E* and *F*, which examined NFAT activation as a function of the magnitude of depolarization (and $[Ca^{2+}]_i$ elevation), cells were treated with K^+10, K^+15, K^+20,

or K^+25 for 12 h. Cells were always lysed 12 h after beginning of the stimulation and subsequently analyzed using the Promega single- or dual-luciferase protocol.

An EGFP-based reporter plasmid (pNFAT-TA-EGFP) was constructed by replacing the luciferase portion of the pNFAT-TA-luciferase construct (Clontech) with the EGFP coding sequence of the pEGFP-N1 construct (Clontech). DRG cultures were transfected with pNFAT-TA-EGFP, 20 h later stimulated with 90 mM KCl, and, after an additional 12 h in culture, were analyzed for EGFP expression in individual DRG neurons using the same fluorescence microscopy setup as described above. EGFP-positive cells were defined by setting the discrimination threshold to 115 arbitrary units (a.u.), which is >3 SDs (SD = 5.6 a.u.) greater than the mean cellular autofluorescence intensity (95.2 a.u.; $n = 21$; determined in untransfected cultures). All measurements were performed using the following identical configurations and parameters: 100 ms exposure; 2×2 binning; $\lambda_{ex} = 475$ (12) nm; $\lambda_{em} = 530$ (50) nm; and 40× oil-immersion objective (NA = 1.35, Olympus).

RT-PCR and real-time RT-PCR analysis. Enriched neuronal DRG cultures were prepared as previously described (Usachev et al., 2002). Total RNA was isolated using the RNase easy mini kit (Qiagen) and reverse transcribed and amplified using the one-step RT-PCR kit (Qiagen) according to the manufacturer's protocols. The following sets of primers specific for rat NFATc1, NFATc2, NFATc3, and NFATc4 were synthesized (Integrated DNA Technology) and used: NFATc1, forward (F), 5′-CAA-CGC-CCT-GAC-CAC-CGA-TAG-3′; NFATc1, reverse (R), 5′-GGC-TGC-CTT-CCG-TCT-CAT-AGT-3′; NFATc2, F, 5′-ACA-TCC-GGG-TGC-CCG-TGA-AAG-T-3′; NFATc2, R, 5′-CTC-GGG-GCA-GTC-TGT-TGT-TGG-ATG-3′; NFATc3, F, 5-CTA-CTG-GTG-GCC-ATC-CTG-TTG-T-3; NFATc3, R, 5-AGC-TCT-TGA-GCA-GAT-CGC-TGA-GAG-CAC-TC-3; NFATc4, F, 5-AAC-ATG-GCT-GCC-AAC-ATT-GA-3; NFATc4, R, 5-CCC-GCT-TGT-TGC-TGT-ACT-CA-3. RT-PCRs were performed (Hybaid PCR Sprint Thermal Cycler) under the following conditions: 50°C for 30 min for reverse transcription, followed by 95°C for 15 min for initial PCR activation and then 95°C for 1 min, 55°C (50°C for NFATc2) for 1 min, and 72°C for 1 min for 30 cycles, and 72°C for 10 min. Amplified transcripts were separated by electrophoresis in 1% gel agarose and detected using ethidium bromide.

To determine the absolute copy number of each NFAT isoform, we performed SYBR green-based real-time RT-PCR. The SYBR green I nucleic acid gel stain (catalog #S7563, Invitrogen) was added to RT-PCRs (one-step RT-PCR kit, Qiagen), which were performed using the Bio-Rad CFX96 system (Bio-Rad). To construct standard curves, the amount of NFAT plasmid DNA (GFP-NFATc1, Addgene plasmid 11101; EGFP-NFATc2, provided by Dr. Rao; GFP-NFATc3, provided by Dr. Iino; EGFP-NFATc4, Addgene plasmid 10961) was measured using a NanoDrop-1000 spectrophotometer (Thermo Scientific), after which each plasmid was serially diluted to copy numbers ranging from 9.4×10^2 to 1.0×10^8 per reaction. The NFAT plasmid dilutions and the NFAT transcripts in the total RNA isolated from neuron-enriched cultured rat DRGs were amplified with the following isoform-specific primer sets: NFATc1, F, 5′-CAT-CAA-CGC-CCT-GAC-CAC-3′, R, 5′-GTG-GTG-CCC-AGG-TCT-TCC-3′, NFATc2, F, 5′-TCT-GCT-GTT-CTC-ATG-GAT-GC-3′, R, 5′-TCA-GGA-CTG-GTC-TTC-CAT-ATC-3′, NFATc3, F, 5′-GAT-CAA-GCT-GCC-ATA-CTA-CCA-3′, R, 5′-CTG-AGA-TCC-AAG-GCC-ATC-ATC-3′, NFATc4, F, 5′-GAG-CAG-CTG-GAG-CTG-AGG-3′, R, 5′-TGT-AGC-CTA-GGA-GCT-TGA- C-3′. The program for the real-time RT-PCR was 50°C for 30 min for reverse transcription, 95°C for 15 min for PCR polymerase activation, and then 94°C for 30 s, 55°C for 30 s, and 72°C for 30 s for 30 cycles. The cycle threshold (Ct) value of each NFAT plasmid dilution was plotted against the logarithm of the corresponding plasmid copy number. Then the standard curves for each NFAT isoform were constructed by a linear regression with plotted points. The absolute copy number of each NFAT isoform was calculated by relating its Ct value to the corresponding standard curve. The specificity of the amplicons was determined by both a melting curve analysis and a 3% agarose gel analysis. The PCR efficiencies were 1.87 ± 0.01 for NFATc1, 1.91 ± 0.02 for NFATc2, 1.85 ± 0.02 for NFATc3, and 1.89 ± 0.01 for NFATc4, as determined by the slope of the standard curve according to the following equation: Efficiency $= 10^{(-1/\text{slope})}$.

Reagents. Fura-2 AM was obtained from Invitrogen; capsaicin, CGP37157, cyclosporin A, and NADA were from Tocris Bioscience; ionomycin was from Calbiochem; FK-506 and oligomycin were from Alomone Laboratories; and leptomycin B was from LC Laboratories. All other reagents were purchased from Sigma.

Results

Characterization of NFAT signaling in rat DRG neurons

Using RT-PCR, we detected the transcripts for NFATc1, NFATc2, NFATc3, and NFATc4 isoforms in DRG neurons (Fig. 1*A*). Further analysis using quantitative real-time RT-PCR showed that NFATc3 transcript predominates among the NFAT isoforms expressed in DRG neurons (Fig. 1*B*) (supplemental Fig. 1, available at www.jneurosci.org as supplemental material). We also examined the transcriptional activity of endogenous NFAT using an NFAT-luciferase expression reporter (Clontech). Depolarization (20 mM KCl) for 2, 6, and 12 h induced a marked increase in the expression of the reporter gene, which depended on the duration of depolarization and was completely abolished by addition of CaN inhibitors cyclosporin A (CsA; 1 μM) (Fig. 1*C*) or FK-506 (200 nM) (Fig. 1*C*).

When activated, NFAT translocates to the nucleus. To further characterize NFAT regulation in DRG neurons, we transfected cells with a plasmid encoding NFATc3 (major NFAT isoform in DRG neurons) fused with a green fluorescent protein (GFP-NFATc3), as previously described (Jackson et al., 2007). Subsequently, DRG neurons were loaded with the Ca^{2+} indicator fura-2, and $[Ca^{2+}]_i$ and GFP-NFATc3 dynamics were monitored simultaneously. Nuclear translocation of NFATc3 was quantified by calculating the ratio of the mean nuclear/cytosolic GFP fluorescence (Fig. 1*E–G*). This approach permits repeated quantitative measurement of NFATc3 dynamics in real time and enables one to relate NFAT localization to changes in $[Ca^{2+}]_i$. GFP-NFATc3 was excluded from the nuclei in the resting state (Fig. 1*D*). Depolarization using K^+90 induced a rapid $[Ca^{2+}]_i$ elevation throughout the cell body, which was followed by nuclear translocation of GFP-NFATc3. Nuclear import of NFATc3 was essentially complete within ~10 min. The return of $[Ca^{2+}]_i$ to baseline levels induced NFATc3 export from the nucleus, and the protein relocated to the cytosol within ~15 min (Fig. 1*E–G*) (supplemental Movie 1, available at www.jneurosci.org as supplemental material).

The CaN inhibitor FK-506 (200 nM) completely blocked depolarization-induced NFAT activation, but had no effect on the $[Ca^{2+}]_i$ transients (Fig. 1*E*) ($n = 6$). The effect of another CaN inhibitor, CsA (5 μM), was virtually identical ($n = 5$; data not shown) to that of FK-506. These data once again emphasize the key role of CaN in mediating the Ca^{2+}-dependent activation and nuclear import of NFAT in DRG neurons. Previous studies showed that activated CaN remains associated with NFAT in the nucleus, which prevents binding of the exportin Crm-1 to NFAT, thereby promoting nuclear retention of NFAT (Zhu and McKeon, 1999). These findings also imply that sustained NFAT activation requires the spread of $[Ca^{2+}]_i$ elevation to the nucleus. It is likely that similar mechanisms are involved in NFAT regulation in DRG neurons. Indeed, we found that the selective Crm-1 inhibitor leptomycin B (100 nM) prevented nuclear export of NFAT even after $[Ca^{2+}]_i$ recovered to baseline levels ($n = 4$) (supplemental Fig. 2, available at www.jneurosci.org as supplemental material).

A sustained activation of CaN requires superoxide dismutase (SOD) to protect CaN from inactivation by superoxide radicals

(O_2^-) (Wang et al., 1996) that are produced in mitochondria in response to strong Ca^{2+} entry (Bito et al., 1996; Hongpaisan et al., 2004). Consistent with this idea, we found that the inhibition of SOD by diethyldithiocarbamic acid (DETC) significantly reduced depolarization-induced nuclear import of NFATc3 in DRG neurons ($n = 11$) (Fig. 1*F*). A free radical scavenger, *N*-acetylcysteine (NAc; 5 mM), prevented the inhibitory effect of DETC on NFATc3 translocation ($n = 7$) (Fig. 1*G*). Interestingly, NAc did not significantly affect depolarization-induced NFATc3 dynamics when applied alone ($n = 9$), suggesting that O_2^- levels were already low in DRG neurons under control conditions, most likely due to the activity of SOD.

Intense electrical stimulation and TRPV1 agonists activate NFAT in DRG neurons

Next, we examined NFAT activation in response to the firing of action potentials. DRG neurons were stimulated using a single train (10 Hz for 10 s) or four trains (15 Hz for 10 s, 60 s apart) of action potentials (Fig. 2*A*,*B*) (supplemental Movie 2, available at www.jneurosci.org as supplemental material). These protocols are consistent with the firing patterns observed in primary afferent fibers in response to thermal or mechanical stimulation *in vivo* (Meyer and Campbell, 1981; Slugg et al., 2000). In addition, similar stimulation protocols were used by others for studying transcription responses in sensory neurons (Fields et al., 1997; Brosenitsch and Katz, 2001; Eshete and Fields, 2001). Action potential stimulation elicited large and long-lasting elevations of $[Ca^{2+}]_i$ in both the cytosol ($[Ca^{2+}]_{cyt}$) and the nucleus ($[Ca^{2+}]_{nuc}$), which were accompanied by a rapid nuclear translocation of NFATc3 (Fig. 2*A*,*B*). Notably, there was only a short (30–40 s) delay between the $[Ca^{2+}]_i$ rise and the initiation of NFAT translocation. The nuclear/cytosolic ratio of GFP-NFATc3 fluorescence was 0.57 ± 0.03 ($n = 16$) in resting cells and increased to the peak values of 1.54 ± 0.13 ($n = 13$; range: 0.82–2.11) and 2.53 ± 0.69 ($n = 3$; range: 1.32–3.72) in response to a single burst and four bursts of action potentials, respectively (Fig. 2*A*,*B*).

A subpopulation of nociceptive sensory neurons expresses the vanilloid receptor TRPV1, which serves as a molecular integrator of pain-producing stimuli, such as noxious heat, protons, and lipid-derived endovanilloids (Caterina and Julius, 2001; Bhave and Gereau, 2004; Lu et al., 2006; Szallasi et al., 2007). The TRPV1 agonist capsaicin (1 μM, 30 s) induced a robust and prolonged increase of both $[Ca^{2+}]_{cyt}$ and $[Ca^{2+}]_{nuc}$ in 12 out of 27 medium- and small-size DRG neurons transfected with GFP-NFATc3. In each of the capsaicin-responsive neurons, the $[Ca^{2+}]_i$ elevation was followed by nuclear import of NFATc3 (Fig. 2*C*). The nuclear/cytosolic GFP-NFATc3 fluorescence ratio was 0.45 ± 0.02 in resting cells and reached the level of 1.84 ± 0.15 ($n = 12$; range: 1.25–2.74) after the capsaicin treatment. An endogenous TRPV1 agonist, *N*-arachidonoyl-dopamine or NADA (Huang et al., 2002), also induced a large and long-lasting $[Ca^{2+}]_i$ increase and the nuclear translocation of NFATc3 ($n = 3$) (Fig. 2*D*). Thus, action potentials and TRPV1 agonists rapidly activate NFATc3 in DRG neurons.

A common feature of the described Ca^{2+} responses is the secondary prolonged $[Ca^{2+}]_i$ plateau phase that follows the initial $[Ca^{2+}]_i$ peak (Fig. 2*A*–*D*). The $[Ca^{2+}]_i$ plateau induced by large Ca^{2+} loads in peripheral and central neurons is mediated by mitochondria that buffer Ca^{2+} influx during stimulation via the uniporter mechanism and subsequently release accumulated Ca^{2+} back into the cytosol via the mitochondrial Na^+/Ca^{2+} exchanger (Miller, 1991; Pivovarova et al., 1999; Friel, 2000; Thayer et al., 2002). During the plateau phase, $[Ca^{2+}]_i$ remained elevated in all parts of the cell body, suggesting a widespread engagement of mitochondria in Ca^{2+} transport (Fig. 2*A*–*D*). We confirmed this using the mitochondrion-targeted Ca^{2+} indicator mtPericam (Nagai et al., 2001) to monitor mitochondrial Ca^{2+} concentration ($[Ca^{2+}]_{mt}$) in response to action potentials ($n = 11$) (Fig. 2*E*) (supplemental Movie 3, available at www.jneurosci.org as supplemental material) and capsaicin ($n = 5$) (Fig. 2*F*). Notably, Ca^{2+} uptake by, and Ca^{2+} release from, mitochondria were observed throughout the cell body, including subplasma membrane areas and the perinuclear region.

Does the described widespread and prolonged $[Ca^{2+}]_i$ plateau contribute to NFAT activation in sensory neurons? To answer this question, we first performed a quantitative analysis of NFAT activation as a function of $[Ca^{2+}]_i$ in DRG neurons.

Quantification of NFAT activation as a function of $[Ca^{2+}]_i$ in DRG neurons

$[Ca^{2+}]_i$ changes and GFP-NFATc3 dynamics were studied simultaneously following a stepwise depolarization by raising extracellular K^+ concentration ($[K^+]_o$) from 5 to 10, 15, 20, and 25 mM, respectively (Fig. 3*A*). As a result, $[Ca^{2+}]_i$ also increased in a stepwise manner. Elevation of $[Ca^{2+}]_i$ to above 200–300 nM triggered NFATc3 import into the nucleus, whereas a decline in $[Ca^{2+}]_i$ to below ~300 nM ($n = 5$) upon repolarization initiated NFATc3 export from the nucleus (Fig. 3*A*).

To perform a more detailed examination of nuclear NFAT import as a function of $[Ca^{2+}]_i$, we used a modified protocol in which neurons were treated for 40–60 min with one of the following high-K^+ solutions: K^+10, K^+15, K^+20, or K^+25 (Fig. 3*B*). The magnitude and the rate of NFAT translocation in each neuron were subsequently analyzed. The results of these experiments are summarized in Figure 3 and in supplemental Figure 3, available at www.jneurosci.org as supplemental material. Specifically, we found that K^+10-induced depolarization triggered nuclear translocation of GFP-NFATc3 in four of six DRG neurons tested, whereas K^+15 evoked GFP-NFATc3 translocation in seven of eight neurons (supplemental Fig. 3*E*, available at www.jneurosci.org as supplemental material). The corresponding $[Ca^{2+}]_i$ peak elevations were 143 ± 30 nM ($n = 6$) and 475 ± 84 nM ($n = 8$) for the K^+10- and K^+15-induced depolarizations, respectively. Stronger stimulations, such as those induced by K^+20- or K^+25-containing solutions, evoked NFAT nuclear import in all DRG neurons examined ($n = 7$ for K^+20 and $n = 5$ for K^+25). Plotting the magnitude of NFATc3 translocation as a function of $[Ca^{2+}]_i$ peak elevation for each individual neuron revealed that $[Ca^{2+}]_i$ increases above ~220 nM were sufficient to induce NFATc3 translocation in all the neurons tested (supplemental Fig. 3*E*, available at www.jneurosci.org as supplemental material). Given that the introduction of an exogenous mobile high-affinity Ca^{2+} buffer such as fura-2 could potentially alter the spatiotemporal characteristics of $[Ca^{2+}]_i$ signals, we repeated analysis of NFATc3 translocation in response to K^+10-, K^+15-, K^+20-, and K^+25-induced depolarizations in DRG neurons that had not been loaded with the indicator. Overall, we found that the magnitudes and the rates of NFATc3 nuclear translocations were similar between fura-2-loaded neurons and those that had not been loaded with the indicator (Fig. 3*C*,*D*).

In smooth muscles, sustained highly localized $[Ca^{2+}]_i$ elevations (persistent Ca^{2+} sparklets) near the sites of Ca^{2+} entry through the L-type Ca^{2+} channels were shown to activate NFATc3 (Nieves-Cintrón et al., 2008). Although we have not

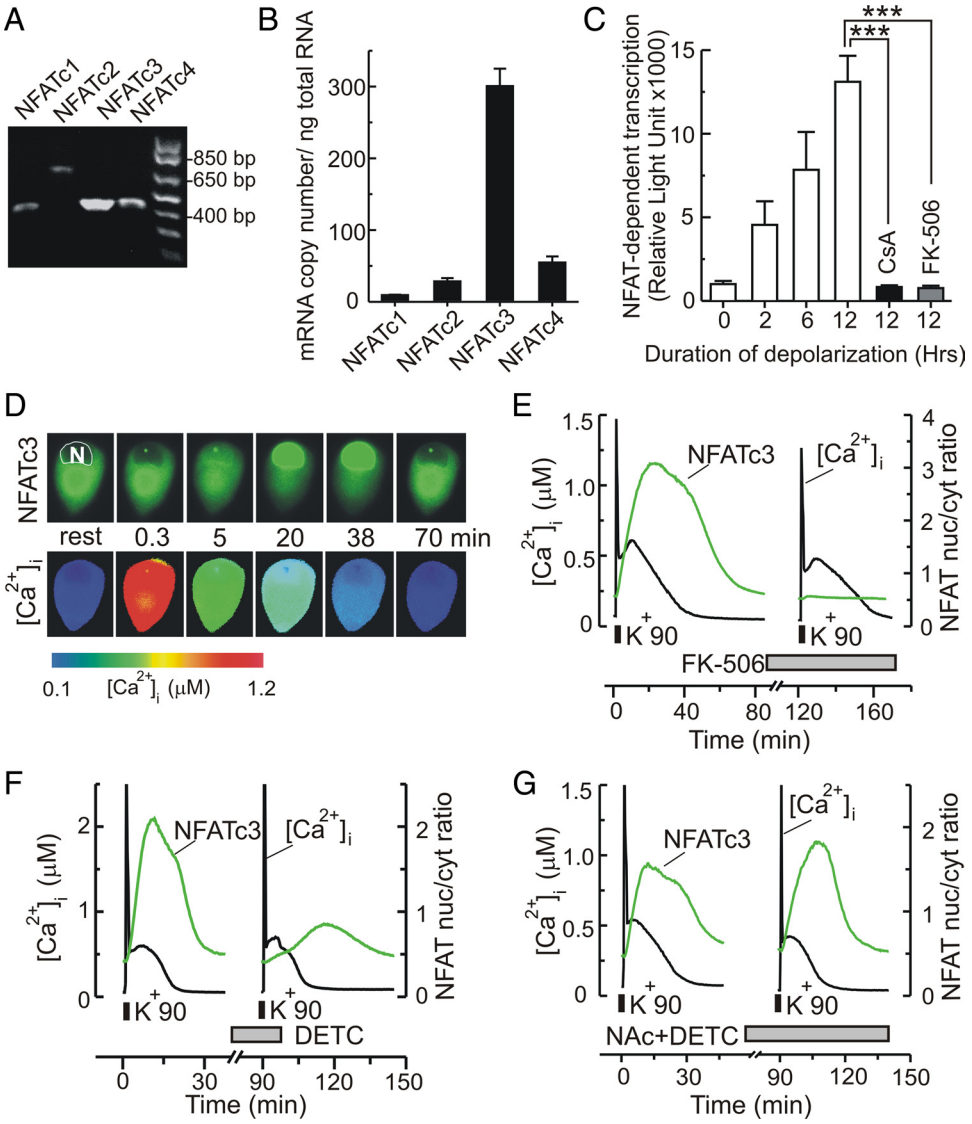

Figure 1. Expression and pharmacological characterization of NFAT in DRG neurons. ***A***, ***B***, RT-PCR (***A***; $n = 3$ independent experiments) and real-time RT-PCR (***B***; $n = 4$ independent experiments) show expression of NFATc1 (also known as NFAT2), NFATc2 (also known as NFAT1), NFATc3 (also known as NFAT4), and NFATc4 (also known as NFAT3) isoforms in DRG neurons, with the highest level of mRNA detected for the NFATc3 isoform. ***C***, Depolarization induces NFAT-mediated luciferase expression in DRG neurons. Cells were either left untreated (control) or stimulated with 20 mM KCl for 2, 6, or 12 h (indicated under the graph) in the absence (white) or presence of the calcineurin inhibitors cyclosporin A (CsA; 1 μM; black) and FK-506 (200 nM; gray). Luciferase expression is shown in relative light units (mean ± SEM). Each data point represents 4–10 independent experiments. ***$p < 0.001$, one-way ANOVA with Bonferroni's *post hoc* test. ***D***, $[Ca^{2+}]_i$ changes and GFP-NFATc3 nuclear translocation were simultaneously monitored in a DRG neuron stimulated with K^+90 (3 min). Images show spatial distribution of GFP-NFATc3 (top) and $[Ca^{2+}]_i$ (bottom, color-coded) either at rest or at various times after stimulation with K^+90. N, Cell nucleus. ***E***, Simultaneous recording of GFP-NFATc3 nuclear import (green) and $[Ca^{2+}]_i$ (black) in DRG neurons stimulated with K^+90 (30 s) in the absence or presence of the calcineurin inhibitor FK-506 (120 min between K^+90-induced depolarizations). Treatment with 200 nM FK-506 prevented nuclear import of NFATc3 but had no effect on the $[Ca^{2+}]_i$ signal. Nuclear translocation of GFP-NFATc3 was quantified by calculating the mean nuclear/cytosolic ratio of GFP fluorescence. ***F***, ***G***, Simultaneous imaging of $[Ca^{2+}]_i$ changes (black) and GFP-NFATc3 nuclear import (green) in response to K^+90-induced depolarization (30 s) in the absence (control) or presence of agents that modulate the intracellular concentration of superoxide radicals (O_2^-). K^+90-induced depolarizations were separated by 90 min. Treatment with the SOD inhibitor diethyldithiocarbamic acid (DETC, 2 mM) strongly reduced nuclear import of NFATc3 evoked by K^+90 ($n = 6$; ***F***), and 5 mM DETC completely blocked NFATc3 translocation ($n = 5$; data not shown). The O_2^- scavenger NAc (5 mM) prevented the inhibitory effect of 2 mM DETC ($n = 7$; ***G***). However, when applied alone, 5 mM NAc did not affect nuclear import of NFATc3 ($n = 9$). To quantify the effects of DETC and NAc on NFATc3 activation, the magnitude of GFP-NFATc3 translocation was calculated as $\Delta R_{NFAT} = R_{peak} - R_{rest}$, where R_{rest} and R_{peak} are the nucleus/cytosol ratios of GFP-NFATc3 at rest and at the maximum of NFATc3 translocation, respectively. For each experiment, the degree of NFATc3 translocation induced by the second K^+90 application ($\Delta R2_{NFAT}$) was normalized to that induced by the first K^+90 pulse ($\Delta R1_{NFAT}$). The $\Delta R2_{NFAT}/\Delta R1_{NFAT}$ ratios were 81 ± 5% for control conditions ($n = 7$; no additional treatments), 44 ± 13% for 2 mM DETC ($n = 6$, $p < 0.05$), 1.3 ± 0.2% for 5 mM DETC ($n = 5$, $p < 0.01$), and 75 ± 7% for 5 mM NAc ($n = 9$, $p > 0.05$); one-way ANOVA with Bonferroni's post-test relative to control. For the combined application of 2 mM DETC plus 5 mM NAc, the $\Delta R2_{NFAT}/\Delta R1_{NFAT}$ ratio was 134 ± 12% ($n = 7$), which is significantly different from the effect of 2 mM DETC applied alone ($p < 0.001$; one-way ANOVA with Bonferroni's post test).

detected Ca^{2+} sparklets in response to depolarization (supplemental Figs. 3 and 4, available at www.jneurosci.org as supplemental material), the possibility that such local events took place in DRG neurons cannot be completely ruled out. If microdomains of highly elevated $[Ca^{2+}]_i$ near the plasma membrane are important for NFAT activation in DRG neurons, then the described high-K^+ depolarization experiments might have overestimated the $[Ca^{2+}]_i$ sensitivity of NFAT. Given these considerations, we further inspected $[Ca^{2+}]_i$ dependence of NFAT activation by using two additional alternative approaches to elevate $[Ca^{2+}]_i$. For the first approach, we examined the Ca^{2+} dependence of GFP-NFATc3 nuclear translocation by inducing

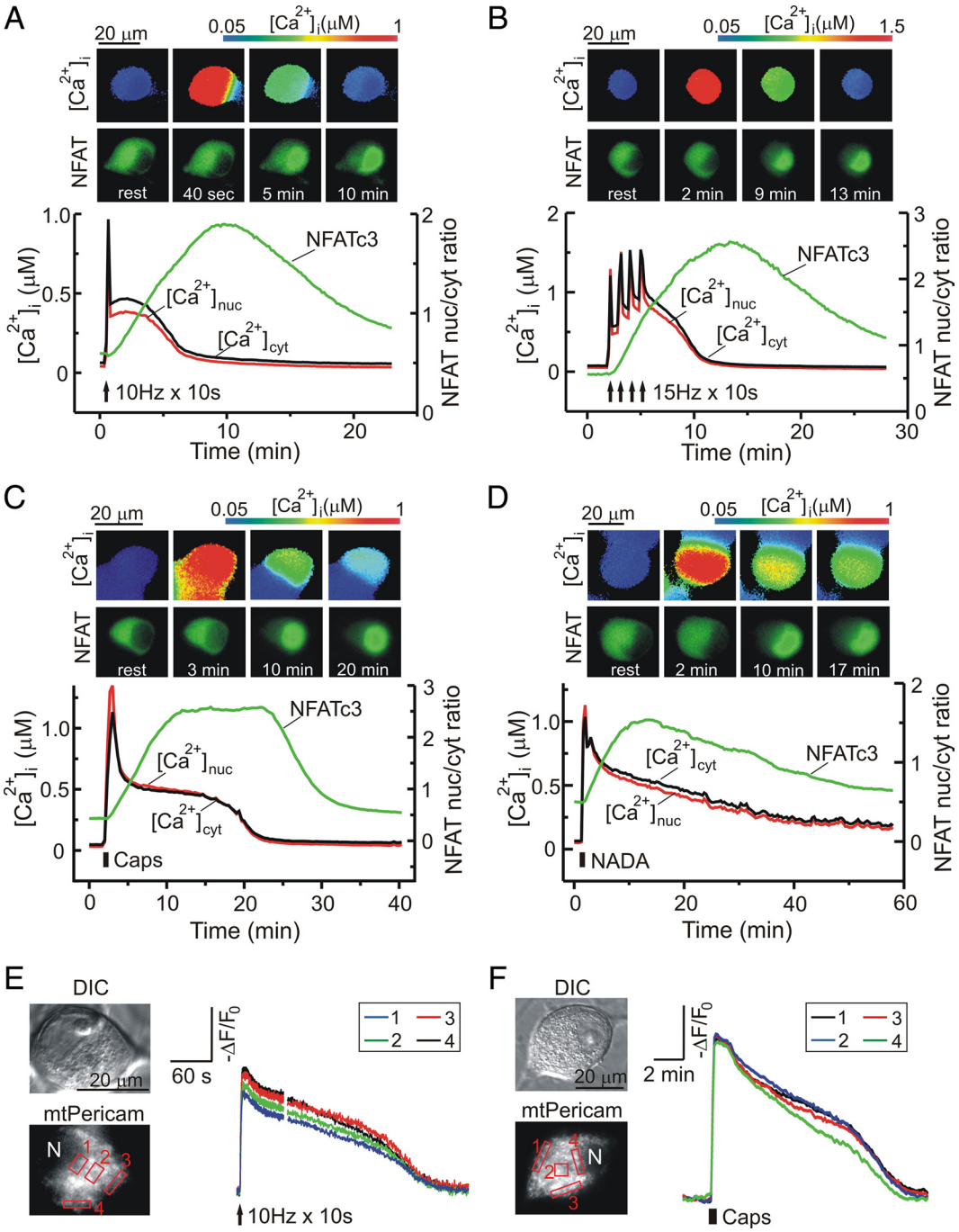

Figure 2. Bursts of action potentials and TRPV1 agonists activate NFAT in DRG neurons. ***A–D***, Simultaneous recording of GFP-NFATc3 movement (green) and $[Ca^{2+}]_i$ changes in the cytosol ($[Ca^{2+}]_{cyt}$; black) and in the nucleus ($[Ca^{2+}]_{nuc}$; red) in response to a single train (arrow; ***A***) or four trains (arrows; ***B***) of action potentials or to the TRPV1 agonists capsaicin (1 μM, 30 s; ***C***) or NADA (5 μM, 30 s; ***D***). Images above the traces show the corresponding distributions of $[Ca^{2+}]_i$ (top; color-coded) and GFP-NFATc3 (bottom) at the time points indicated. $[Ca^{2+}]_i$ images in ***C*** and ***D*** depict both GFP-NFATc3-transfected and untransfected neurons. Action potentials were evoked using extracellular field stimulation (Usachev and Thayer, 1999). ***E***, ***F***, Changes in mitochondrial Ca^{2+} concentration ($[Ca^{2+}]_{mt}$) evoked by action potentials (***E***, 10 Hz for 10 s; arrow) or capsaicin (***F***, 1 μM, 30 s; black bar) in an mtPericam-transfected DRG neuron. Images were collected at the sampling rate of 10 Hz for the first 60 s and 2 Hz for the rest of the recording (separated by the break in the trace) in ***E***, and at 0.2 Hz for the recording in ***F***. Differential interference contrast (DIC; top) and mtPericam fluorescence (bottom; $\lambda_{ex} = 410$ nm) images of the studied cell are shown on left. Color- and number-coded traces show $[Ca^{2+}]_{mt}$ changes in the areas outlined by red boxes. N, Nuclear region.

Ca^{2+} leak from the endoplasmic reticulum (ER) Ca^{2+} stores with a specific SERCA (sarco-ER Ca^{2+}-ATPase) inhibitor, cyclopiazonic acid (CPA; 5 μM) (Usachev and Thayer, 1999; Lu et al., 2006; Usachev et al., 2006). CPA-induced Ca^{2+} leak from the ER Ca^{2+} stores is a slow process (compared with Ca^{2+} release mediated by ryanodine or inositol triphosphate receptors) (Camello et al., 2002) and is unlikely to be associated with the generation of $[Ca^{2+}]_i$ "hot spots," which requires both high-conductance Ca^{2+} channels and a steep Ca^{2+} gradient. Indeed, CPA induced a gradual and homogenous $[Ca^{2+}]_i$ elevation throughout the cell (supplemental Fig. 5*A*, available at www.jneurosci.org as supplemental material) (Usachev et al., 2006). We found that 5 μM CPA induced nuclear translocation of GFP-NFATc3 in 12 of 21 DRG neurons tested (supplemental Fig. 5, available at www.jneurosci.org as supplemental material). For the responding neurons in which CPA triggered nuclear import of NFAT, the peak

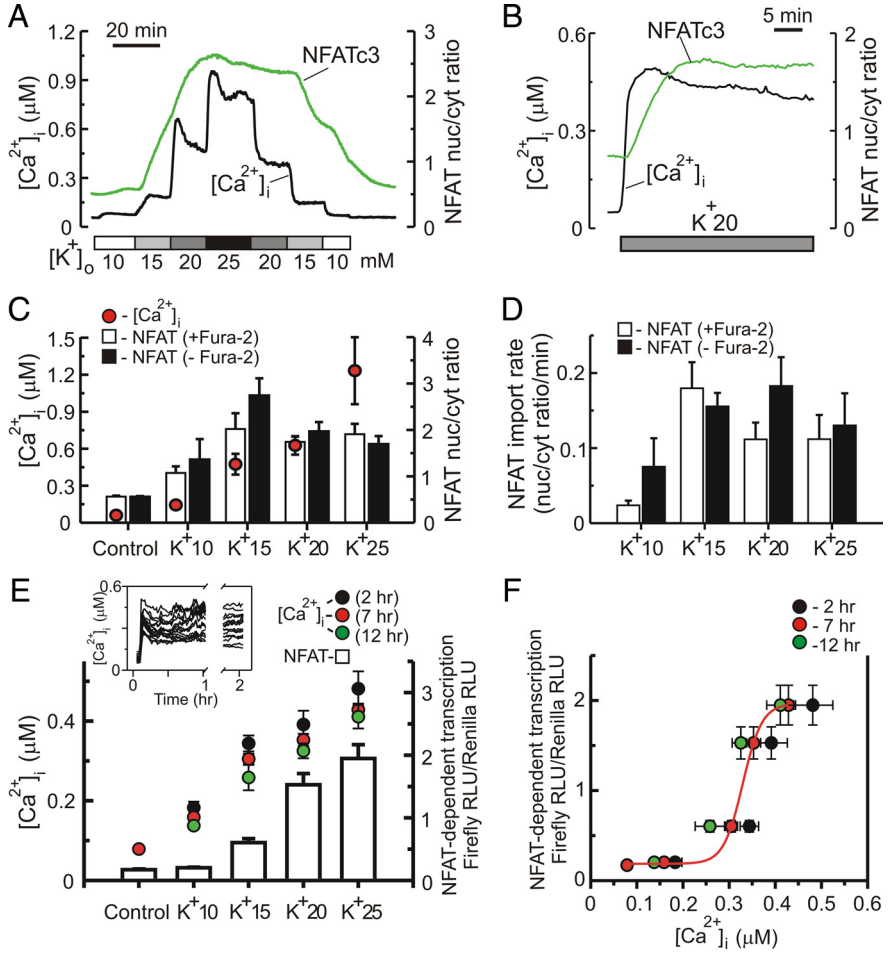

Figure 3. Quantification of NFAT activation as a function of $[Ca^{2+}]_i$ in DRG neurons. ***A***, Simultaneous recording of GFP-NFATc3 nuclear import (green) and $[Ca^{2+}]_i$ changes (black) in a DRG neuron in response to incremental depolarization caused by raising the extracellular K^+ concentration ($[K^+]_o$) from 5 mM to 10, 15, 20, and 25 mM. K^+10-, K^+15-, K^+20-, and K^+25-containing solutions were supplemented with the L-type Ca^{2+} channel agonist BayK8644 (1 μM). ***B***, $[Ca^{2+}]_i$ elevation (black) and nuclear translocation of GFP-NFATc3 (green) in a DRG neuron were induced by prolonged application of 20 mM KCl (K^+20; gray bar) combined with 1 μM BayK8644. DRG neurons were transfected with GFP-NFATc3 and subsequently loaded with fura-2, as described in Materials and Methods. ***C***, Plot summarizes depolarization-induced peak $[Ca^{2+}]_i$ elevations (red circles; mean ± SEM) and the maximal GFP-NFATc3 nuclear/cytosolic ratios attained upon NFATc3 translocation to the nucleus (open vertical bars; mean ± SEM). Cells were stimulated with K^+10-, K^+15-, K^+20-, or K^+25-containing solutions using protocols similar to that described for ***B***. Black bars summarize the maximal GFP-NFATc3 nuclear/cytosolic ratios achieved upon NFATc3 translocation to the nucleus in similar experiments, with the exception that DRG neurons were not loaded with fura-2 (− Fura-2). ***D***, Quantification of the rate of GFP-NFATc3 nuclear import in response to K^+10-, K^+15-, K^+20-, or K^+25-induced depolarizations. Data were obtained from the experiments like that shown in ***B*** using DRG neurons that either were loaded (empty bars) or were not loaded (black bars) with fura-2. The rate was determined by fitting the initial 5 min of the NFATc3 response with a linear function and by calculating its slope. Depolarizations using K^+10-, K^+15-, K^+20-, or K^+25-containing solutions are indicated under the plots. ***E***, NFAT-mediated expression of luciferase was induced by 10, 15, 20, or 25 mM KCl for 12 h and was analyzed using the Promega dual-luciferase protocol (white bars; mean ± SEM). Each bar represents 3–24 independent experiments. In parallel experiments, $[Ca^{2+}]_i$ changes were induced by 10, 15, 20, or 25 mM KCl under similar conditions (cell culture medium supplemented with 20 mM HEPES, pH = 7.4, temperature = 37°C). For both sets of experiments, K^+10-, K^+15-, K^+20-, and K^+25-containing solutions were supplemented with 1 μM BayK8644. $[Ca^{2+}]_i$ measurements were taken after 2 (black circles), 7 (red circles), or 12 (green circles) h of treatment using the corresponding high-K^+-containing buffers. Each point represents 23–103 neurons. Inset, Representative $[Ca^{2+}]_i$ recording from multiple DRG neurons in the presence of 15 mM KCl. ***F***, NFAT reporter expression is plotted as a function of the $[Ca^{2+}]_i$ level using data from ***E***. For each depolarization condition, NFAT-luciferase expression is plotted versus three $[Ca^{2+}]_i$ measurements that were taken at 2 (black), 7 (red), and 12 (green) h after the beginning of high-K^+ stimulation. Data points were fitted with sigmoid function (smooth curve) using Sigma Plot 9.1 software.

$[Ca^{2+}]_i$ elevation was 130 ± 10 nM (n = 12; range: 100–210 nM); for nonresponding neurons, the peak of the CPA-induced $[Ca^{2+}]_i$ rise was 86 ± 5 nM (n = 9; range: 55–105 nM).

For the second approach, we examined nuclear translocation of NFATc3-GFP in response to $[Ca^{2+}]_i$ increases induced by the Ca^{2+} ionophore ionomycin (10 μM) (supplemental Fig. 6, available at www.jneurosci.org as supplemental material). To limit the $[Ca^{2+}]_i$ rise anywhere in the cell, we set the extracellular Ca^{2+} concentration to either ~170 or 255 nM by mixing 5 mM EGTA with either 4.3 or 4.4 mM $CaCl_2$, respectively, in the extracellular buffer (see Materials and Methods for details). We also added 1 mM La^{3+} to the extracellular solution to block Ca^{2+} extrusion from the cells (Usachev et al., 1993). Since ionomycin can also release Ca^{2+} from the ER Ca^{2+} stores, DRG neurons were pretreated with 5 μM CPA for at least 30 min to deplete intracellular Ca^{2+} stores before the application of ionomycin and La^{3+}. Under these conditions, the protonophore FCCP (*p*-trifluoromethoxyphenylhydrazone) (1 μM) did not induce any increase in $[Ca^{2+}]_i$ (n = 6, data not shown), suggesting that mitochondria were nearly empty. As shown in supplemental Figure 6, *A* and *B*, available at www.jneurosci.org as supplemental material, treating neurons with the combination of ionomycin and La^{3+} essentially clamped $[Ca^{2+}]_i$ at the expected levels set by the extracellular Ca^{2+} concentration. More importantly, these ionomycin-induced $[Ca^{2+}]_i$ elevations were sufficient to trigger nuclear import of NFATc3 in all DRG neurons tested (n = 17) (supplemental Fig. 6, available at www.jneurosci.org as supplemental material).

Thus, three different approaches to increase $[Ca^{2+}]_i$—high-K^+ depolarization, CPA application, and ionomycin/La^{3+} treatment—produced similar results, demonstrating the $[Ca^{2+}]_i$ elevation to 200–300 nM is sufficient to evoke nuclear translocation of NFAT in DRG neurons.

To examine the $[Ca^{2+}]_i$ dependence of the transcriptional activity mediated by the endogenous NFATc proteins, we transfected DRG neurons with the NFAT-luciferase (firefly) reporter gene. Cells were stimulated by elevating $[K^+]_o$ to 10, 15, 20, or 25 mM for 12 h, and luciferase activity was subsequently analyzed [firefly relative light units (RLU)]. The activity of firefly luciferase was normalized to the activity of cotransfected constitutively expressed *Renilla* luciferase (*Renilla* RLU). $[K^+]_o$ elevation to 15 mM and higher produced a robust increase in the expression of the NFAT-luciferase reporter (Fig. 3*E*). In parallel experiments, we also measured the corresponding changes in $[Ca^{2+}]_i$ induced by prolonged elevation of $[K^+]_o$ under conditions similar to those used for the NFAT-luciferase reporter assays (Fig. 3*E*) (supplemental Fig. 4, available at www.jneurosci.org as supplemental material). $[Ca^{2+}]_i$ measurements

were made at 2, 7, and 12 h after the beginning of high-K^+ stimulation. Subsequently, NFAT-luciferase activity was plotted as a function of $[Ca^{2+}]_i$, which revealed a very steep $[Ca^{2+}]_i$ dependence of the NFAT-mediated transcription response in sensory neurons (Fig. 3*F*).

Taken together, these data indicate that NFAT activation in DRG neurons requires an elevation of $[Ca^{2+}]_i$ to >200–300 nM, which is similar to or lower than the $[Ca^{2+}]_i$ levels attained during the $[Ca^{2+}]_i$ plateau phase described in Figure 2.

Depolarization-induced NFAT activation depends on mitochondrial Ca^{2+} cycling

Next, we examined the role of mitochondrial Ca^{2+} uptake/release in the regulation of NFAT. DRG neurons were stimulated by two 30 s pulses of 90 mM KCl separated by a 90 min interval, which enabled eliciting highly reproducible $[Ca^{2+}]_i$ responses with a characteristic $[Ca^{2+}]_i$ plateau phase and also allowed repeated activation of NFAT in the same cell (Fig. 4*A*). First, we used this paired-pulse protocol to examine the effect of the electron chain inhibitor antimycin A1 (1 μM), which depolarizes mitochondria and blocks mitochondrial Ca^{2+} uptake (Nicholls and Budd, 2000). To prevent ATP depletion via the reversal mode of the mitochondrial F_oF_1 ATP synthase (Nicholls and Budd, 2000), we always used antimycin together with the ATP synthase inhibitor oligomycin (5 μM). In the presence of oligomycin, glycolysis maintains the ATP levels in cultured neurons for tens of minutes after the dissipation of electrochemical gradient (Nicholls and Budd, 2000) without impairment of ATP-dependent Ca^{2+} transport (Usachev et al., 2002) or cell viability (Budd and Nicholls, 1996).

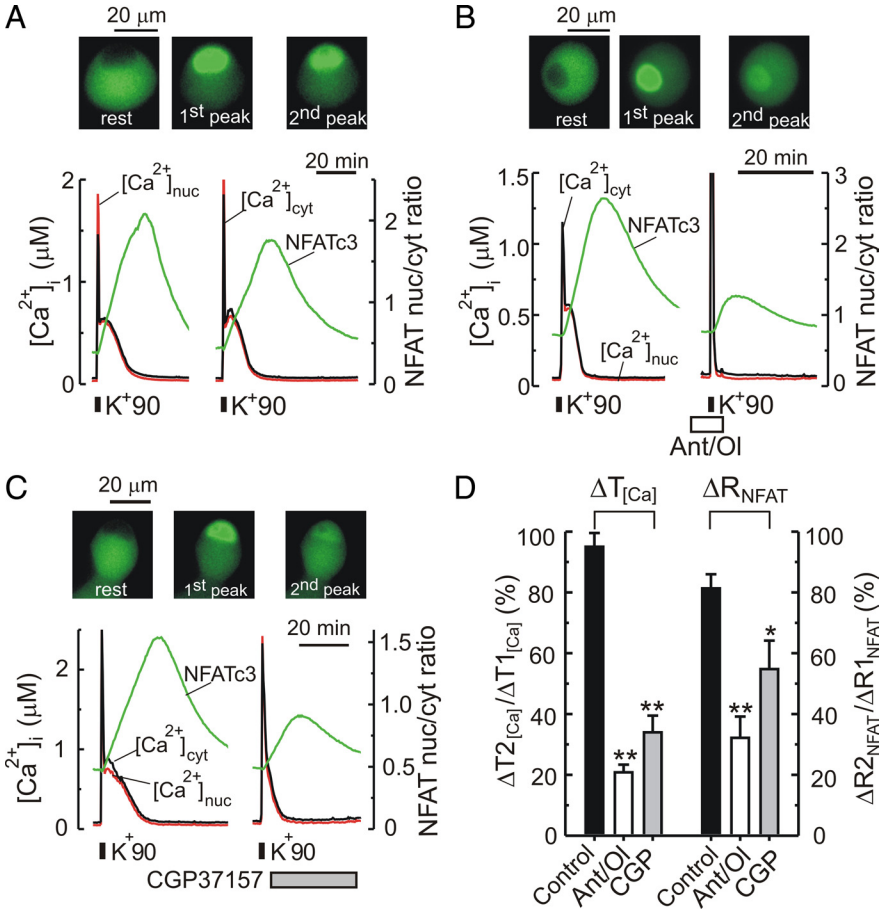

Figure 4. Mitochondria facilitate NFAT activation induced by strong depolarization. ***A–C***, Combined monitoring of GFP-NFATc3 (green) translocation and $[Ca^{2+}]_i$ changes in the cytosol ($[Ca^{2+}]_{cyt}$; black) and in the nucleus ($[Ca^{2+}]_{nuc}$; red) in response to two subsequent K^+90-induced depolarizations (30 s, 90 min apart). In ***B*** and ***C***, DRG neurons were treated with either 1 μM antimycin and 5 μM oligomycin (***B***; Ant/Ol; white bar; 10 min pretreatment) or 10 μM CGP37157 (***C***; gray bar) during the second depolarization. Images above the trace show GFP-NFATc3 distribution at rest and at the peak of NFATc3 nuclear translocation during each depolarization. ***D***, Summary of the effects of the Ant/Ol and CGP37157 treatments on the magnitude of NFATc3 translocation ($\Delta R_{NFAT} = R_{peak} - R_{rest}$, where R_{rest} and R_{peak} are GFP-NFATc3 nuclear/cytosolic ratios at rest and at the maximum of NFATc3 translocation, respectively) and on the duration of the $[Ca^{2+}]_i$ responses ($\Delta T_{[Ca]}$; calculated at the 250 nM $[Ca^{2+}]_i$) in experiments such as those described in ***A–C***. The effects were quantified by calculating the $\Delta R2_{NFAT}/\Delta R1_{NFAT}$ and $\Delta T2_{[Ca]}/\Delta T1_{[Ca]}$ ratios in control experiments (black bars; no additional treatment) and in experiments in which the cells were treated with either Ant/Ol (white bars) or CGP37157 (gray bars) during the second depolarization. *$p < 0.05$, **$p < 0.01$, one-way ANOVA with Bonferroni's *post hoc* test.

Combined treatment with antimycin and oligomycin (Ant/Ol) increased the amplitude of the $[Ca^{2+}]_i$ response and eliminated the $[Ca^{2+}]_i$ plateau phase in both the cytosol and the nucleus (Fig. 4*A*,*B*). More importantly, this blockade of mitochondrial Ca^{2+} uptake markedly decreased nuclear translocation of NFATc3 (Fig. 4*B*). To quantify the Ant/Ol effect on NFATc3 activation, we calculated the magnitude of GFP-NFATc3 translocation induced by K^+90 as $\Delta R_{NFAT} = R_{peak} - R_{rest}$, where R_{rest} and R_{peak} are the nucleus/cytosol ratios of GFP-NFATc3 at rest and at the maximum of NFATc3 translocation, respectively. For each paired-pulse experiment, the degree of NFATc3 translocation induced by the second K^+90 application ($\Delta R2_{NFAT}$) was normalized to that induced by the first K^+90 pulse ($\Delta R1_{NFAT}$). We found that $\Delta R2_{NFAT}$ was 81 ± 5% of $\Delta R1_{NFAT}$ ($n = 7$) under control conditions (Fig. 4*A*) and that it was dramatically decreased by the Ant/Ol treatment ($\Delta R2_{NFAT}/\Delta R1_{NFAT}$ = 32 ± 7%; $n = 5$; $p < 0.01$) (Fig. 4*B*,*D*).

We also performed control experiments (supplemental Fig. 7, available at www.jneurosci.org as supplemental material), in which the duration of a small (<300–500 nM) $[Ca^{2+}]_i$ elevation was set by the duration of a mild depolarization (15 mM KCl, 20 min), independent of mitochondria. Indeed, $[Ca^{2+}]_i$ rapidly returned to the basal levels upon the washout of the K^+15 solution (supplemental Fig. 7*A*, available at www.jneurosci.org as supplemental material), and the duration of the $[Ca^{2+}]_i$ response was not changed by the Ant/Ol treatment (supplemental Fig. 7*B*, available at www.jneurosci.org as supplemental material). Notably, for this protocol NFATc3 translocation was not affected by the combined addition of 1 μM antimycin and 5 μM oligomycin (supplemental Fig. 7*C*, available at www.jneurosci.org as supplemental material), suggesting that these drugs did not affect NFAT transport itself downstream of the $[Ca^{2+}]_i$ elevation.

Another way to disrupt mitochondrial Ca^{2+} cycling is to block Ca^{2+} release from mitochondria, which is mediated by the mitochondrial Na^+/Ca^{2+} exchanger in neurons (David, 1999; Colegrove et al., 2000; Thayer et al., 2002; García-Chacón et al.,

2006; Medvedeva et al., 2008). Therefore we tested the effect of the exchange inhibitor CGP37157 on NFATc3 translocation in DRG neurons using the paired-pulse protocol described above. By monitoring $[Ca^{2+}]_{mt}$ in mtPericam-transfected neurons, we confirmed the ability of CGP37157 to effectively and reversibly block Ca^{2+} release from mitochondria in our system (supplemental Fig. 8, available at www.jneurosci.org as supplemental material). Given that CGP37157 can interfere with depolarization-induced Ca^{2+} influx (Baron and Thayer, 1997), this agent was applied after washing out the K^+90-containing solution. Treatment with 10 μM CGP37157 eliminated the $[Ca^{2+}]_i$ plateau phase, in both the cytosol and the nucleus, and markedly suppressed nuclear translocation of NFATc3 (Fig. 4*C*,*D*). The $\Delta R2_{NFAT}/\Delta R1_{NFAT}$ ratio was reduced from 81 ± 5% ($n = 7$) in control to 55 ± 9% ($n = 7$; $p < 0.05$) (Fig. 4*D*).

We also examined the role of mitochondria in the regulation of other NFAT isoforms expressed in DRG neurons, such as NFATc1, NFATc2, and NFATc4 (Fig. 1*A*,*B*) (Jung and Miller, 2008), using approaches similar to those described for the NFATc3 isoform. Supplemental Figure 9, available at www.jneurosci.org as supplemental material, shows simultaneous recording of $[Ca^{2+}]_i$ and EGFP-NFATc1 (*A–C*), EGFP-NFATc2 (*D–F*), or EGFP-NFATc4 (*G*) in individual DRG neurons. K^+90-induced depolarization (30 s) triggered rapid nuclear translocation of NFATc1 and NFATc2 (supplemental Fig. 9*A*,*D*, available at www.jneurosci.org as supplemental material). However only minute nuclear import of NFATc4 was observed in response to depolarization, even after stimulating cells by three 3 min applications of 90 mM KCl (supplemental Fig. 9*G*, available at www.jneurosci.org as supplemental material). It is possible that NFATc4 is preferentially activated by NGF in DRG neurons (Groth et al., 2007). As for NFATc3, blockade of mitochondrial Ca^{2+} uptake or release strongly reduced nuclear translocation of both NFATc1 and NFATc2 (supplemental Fig. 9, available at www.jneurosci.org as supplemental material).

Taken together, these data demonstrate that disruption of mitochondrial Ca^{2+} cycling by blocking either Ca^{2+} uptake or release strongly suppresses the depolarization-induced nuclear import of NFAT in DRG neurons. These experiments also emphasize the capability of mitochondria to adjust the size and duration of the Ca^{2+} response to suit the activation requirements of calcineurin and the transcription factor NFAT.

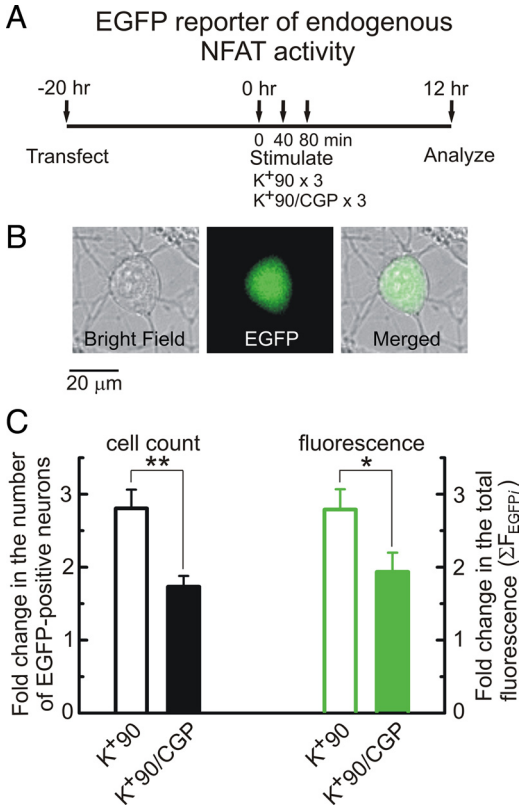

Figure 5. Mitochondrial Ca^{2+} release facilitates transcriptional response mediated by endogenous NFAT. ***A***, Description of the experimental timeline. DRG neurons were transfected with the NFAT-EGFP reporter construct and stimulated 20 h later using three K^+90 depolarizations (3 min each, 40 min apart) either without (K^+90) or with (K^+90/CGP) additional treatment by CGP37157. CGP37157 (3 μM) was applied for 32 min between the stimuli (with 5 min wash before a sequential K^+90 depolarization). EGFP-positive DRG neurons were counted and analyzed after additional 12 h in culture. ***B***, Bright-field (left), fluorescent (middle), and merged (right) images of a DRG neuron transfected with the NFAT-EGFP reporter and stimulated with 90 mM KCl. The images were taken 12 h after the stimulation. ***C***, Summary of the CGP37157 effects on depolarization-induced EGFP expression quantified by counting the number of EGFP-positive DRG neurons (black) and the total EGFP fluorescence in these neurons (green). The numbers of cells (or total EGFP fluorescence) for the K^+90 and K^+90/CGP treatments were normalized to that obtained from untreated control cells for each culture preparation ($n = 6$). $^*p < 0.05$, $^{**}p < 0.01$, Student's *t* test.

Mitochondria facilitate transcription mediated by the endogenous NFATc proteins in DRG neurons

Having established that mitochondria contribute to the nuclear translocation of NFAT isoforms, we tested whether transcription mediated by the endogenous NFATc proteins also depends on these organelles. To rule out a potential contribution of non-neuronal cells that are also present in DRG cultures, a single-cell NFAT reporter assay was performed in these experiments. For this method, cells were transfected with an NFAT-EGFP reporter that enables monitoring NFAT-dependent expression of EGFP in single identified DRG neurons. DRG cultures were stimulated using three applications of K^+90 (90 mM KCl, 3 min, 40 min between applications), and 12 h later, EGFP expression was quantified in individual DRG neurons (Fig. 5*A*,*B*) by two methods: (1) counting the number of EGFP-positive cells (Fig. 5*C*, black bars), and (2) calculating the total EGFP fluorescence in all EGFP-positive cells (ΣF_{EGFPi}) (Fig. 5*C*, green bars). We chose to use CGP37157 to disrupt mitochondrial Ca^{2+} cycling in these experiments because, in contrast to the effects of Ant/Ol, those of CGP37157 are rapidly reversed upon drug removal (Medvedeva et al., 2008) (supplemental Fig. 8, available at www.jneurosci.org as supplemental material), which enables treatments of specified duration. CGP37157 (3 μM) was applied for 32 min immediately after K^+90 removal. K^+90 depolarization increased the number of EGFP-positive DRG neurons and the total EGFP fluorescence by ~2.8-fold compared with those in control (unstimulated) cells (Fig. 5*C*). Inhibition of mitochondrial Ca^{2+} release by CGP37157 significantly reduced both the number of EGFP-positive neurons and the total EGFP fluorescence (Fig. 5*C*) ($n = 6$ independent experiments). In contrast, CGP37157 had no effect on the number of EGFP-expressing neurons transfected with constitutive EGFP that is controlled by the CMV promoter ($n = 3$ independent experiments; data not shown), indicating that the CGP37157 effect is not due to toxicity.

The effect of mitochondria on NFAT activation depends on the Ca^{2+} extrusion mechanisms in DRG neurons

Next, we tested the involvement of mitochondria in NFAT activation by bursts of action potentials or TRPV1 agonist using a

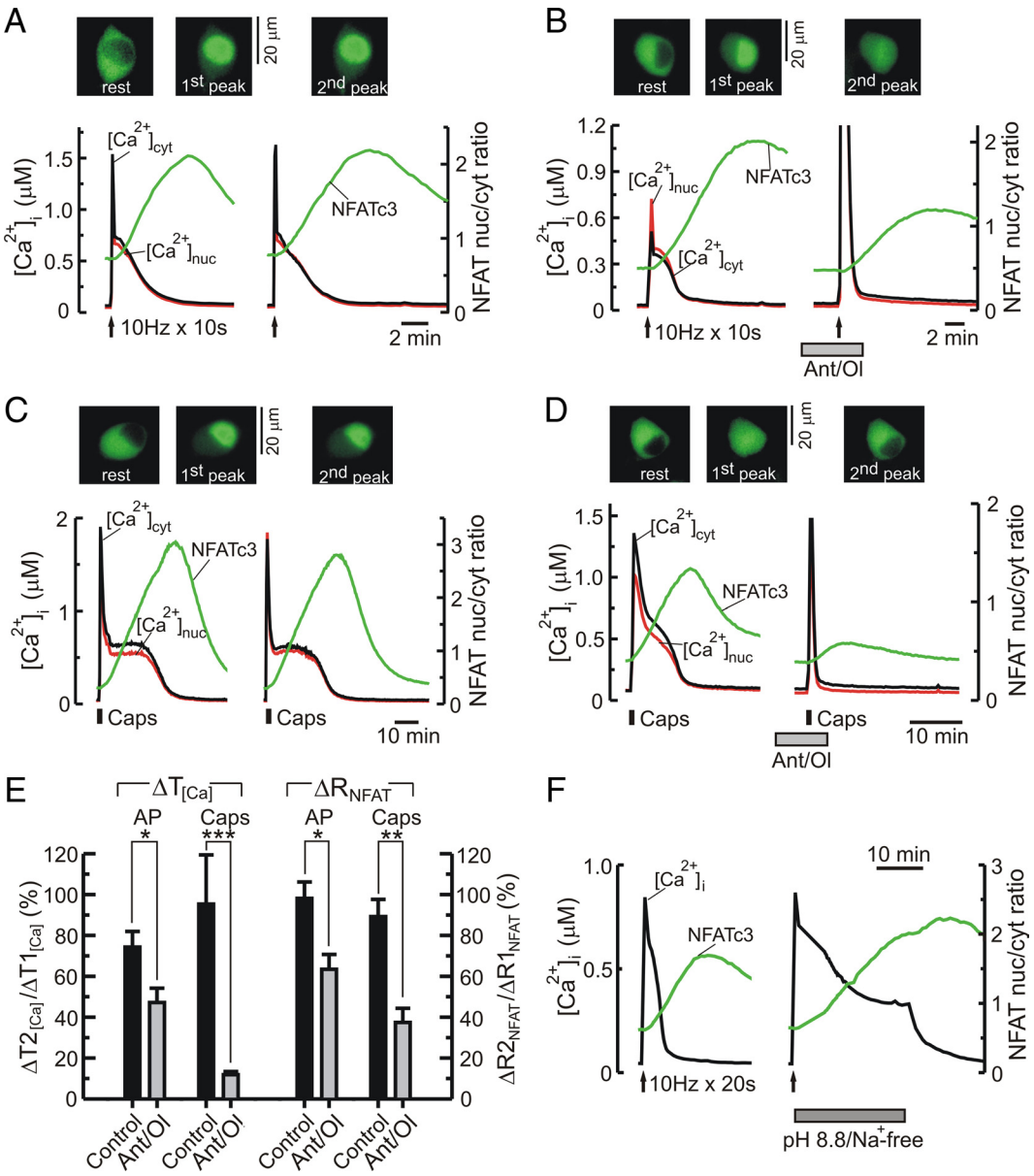

Figure 6. Mitochondria facilitate NFATc3 activation by action potentials and TRPV1 agonist. ***A–D***, Simultaneous recording of GFP-NFATc3 nuclear import (green) and $[Ca^{2+}]_i$ changes in the cytosol ($[Ca^{2+}]_{cyt}$; black) and nucleus ($[Ca^{2+}]_{nuc}$; red) in response to sequential applications of either trains of action potentials (10 Hz for 10 s, 90 min apart; arrows; ***A*** and ***B***) or capsaicin (200 nM, 30 s, 90 min apart; black bars; ***C*** and ***D***). Action potentials were generated using extracellular field stimulation (Usachev and Thayer, 1999). Mitochondrial Ca^{2+} uptake was blocked by applying 1 μM antimycin and 5 μM oligomycin (Ant/Ol; gray bars; ***B*** and ***D***). ***E***, Quantification of the effects of Ant/Ol (gray) on NFATc3 nuclear import ($\Delta R2_{NFAT}/\Delta R1_{NFAT}$) and on the duration ($\Delta T2_{[Ca]}/\Delta T1_{[Ca]}$) of the $[Ca^{2+}]_i$ responses induced by action potentials (AP) or capsaicin (Caps) as described for Figure 4*D*. *$p < 0.05$, **$p < 0.01$, ***$p < 0.001$, Student's *t* test. ***F***, The effect of blocking Ca^{2+} extrusion via PMCA and Na^+/Ca^{2+} exchanger (NCX) on $[Ca^{2+}]_i$ changes (black) and nuclear import of GFP-NFATc3 (green) induced by trains of action potentials (10 Hz for 20 s; arrows; 30 min apart). PMCA and NCX were blocked by raising pH to 8.8 and removing Na^+ (replaced with choline) in the extracellular solution, respectively. This modified extracellular solution was applied after the end of electrical stimulation (gray bar).

paired-pulse protocol similar to that described in Figure 4. Repeated stimulation by either a train of action potentials (10 Hz, 10 s) (Fig. 6*A*,*B*) or the TRPV1 agonist capsaicin (200 nM, 30 s) (Fig. 6*C*,*D*) evoked $[Ca^{2+}]_i$ and NFATc3 responses of reproducible size and duration (Fig. 6*A*,*C*). Treating cells with 1 μM antimycin and 5 μM oligomycin eliminated the $[Ca^{2+}]_i$ plateau and increased the peak $[Ca^{2+}]_i$ elevation. Blockade of mitochondrial Ca^{2+} uptake also markedly reduced the nuclear translocation of NFATc3 for both stimulation protocols (Fig. 6*A*–*E*).

The height and the duration of $[Ca^{2+}]_i$ plateau are defined by the balance between mitochondrial Ca^{2+} release and Ca^{2+} clearance (Colegrove et al., 2000). It is conceivable that factors that affect the Ca^{2+} extrusion machinery also modulate the plateau duration and the degree of NFAT activation in neurons. To test this idea, we blocked plasma membrane Na^+/Ca^{2+} exchange (NCX) by removing extracellular Na^+ (Herrington et al., 1996; Lu et al., 2006) and the activity of the plasma membrane Ca^{2+}-ATPase (PMCA) by raising the extracellular pH to 8.8 (Schwiening et al., 1993; Usachev et al., 2002). This combined treatment essentially stalled $[Ca^{2+}]_i$ recovery for as long as Ca^{2+} extrusion remained inhibited (Fig. 6*F*), and return to the normal extracellular buffer rapidly restored $[Ca^{2+}]_i$ recovery to the baseline level. Notably, the extension of the $[Ca^{2+}]_i$ plateau achieved by inhibiting NCX and PMCA also markedly enhanced nuclear import of NFATc3 ($n = 5$), as predicted by our hypothesis.

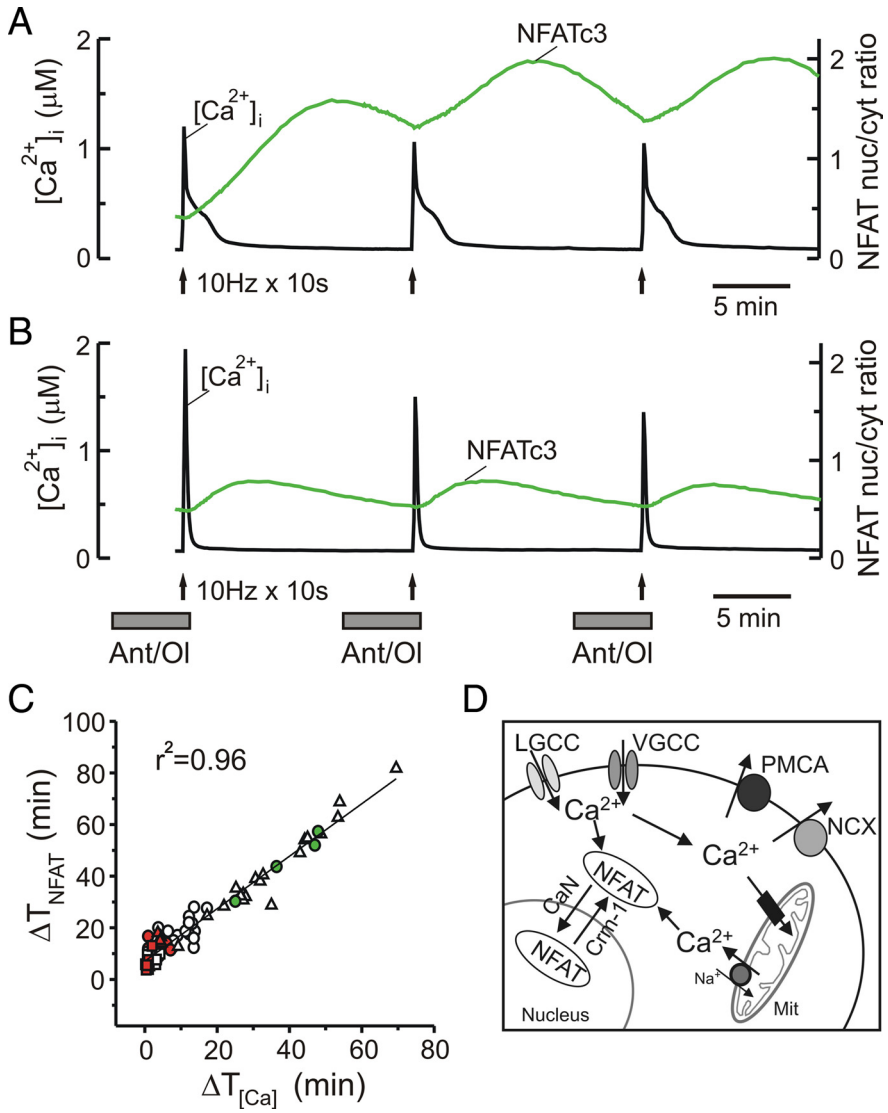

Figure 7. Mitochondria facilitate temporal summation of repetitive electrical activity by NFAT. ***A***, ***B***, Nuclear import of GFP-NFATc3 (green) and $[Ca^{2+}]_i$ elevations (black) were evoked by repetitive trains of action potentials (10 Hz for 10 s, arrows). ***B***, Cells were treated with 1 μM antimycin and 5 μM oligomycin (Ant/Ol; gray bars). ***C***, The extent of GFP-NFATc3 nuclear translocation (ΔT_{NFAT}; time between the initiation of NFATc3 nuclear import and export) was plotted as a function of the duration of $[Ca^{2+}]_i$ elevation (calculated at the 250 nM $[Ca^{2+}]_i$ level) for different stimulation protocols and pharmacological treatments. Squares, triangles, and circles indicate stimulation by action potentials, capsaicin, or 90 mM KCl, respectively. Empty symbols indicate control (no treatment); experiments involving inhibition of mitochondrial Ca^{2+} transport or Ca^{2+} extrusion are denoted by red or green symbols, respectively. Points were fitted with a linear function using Sigma Plot 9.1 software. ***D***, Model summarizes the role of mitochondria in the regulation of NFAT nuclear translocation in neurons that is triggered by Ca^{2+} influx via voltage- or ligand-gated Ca^{2+} channels (VGCC and LGCC, respectively). By steadily releasing Ca^{2+} accumulated during neuronal stimulation, mitochondria markedly extend the elevation in $[Ca^{2+}]_i$ required for NFAT activation beyond the short duration of stimulation.

Mitochondria facilitate the function of NFAT as a nuclear integrator of repetitive neuronal activity

The nuclear export of NFAT occurs with a substantial delay following termination of the $[Ca^{2+}]_i$ signal. As a result, repetitive $[Ca^{2+}]_i$ spikes can lead to temporal summation of NFAT responses within the nucleus, enabling NFAT to function as "a working memory of Ca^{2+} signals" (Tomida et al., 2003). In sympathetic neurons, $[Ca^{2+}]_i$ transients induced by repetitive frequent bursts of action potentials (50 s between the bursts) led to summation and accumulation of NFATc1 in the nucleus (Hernández-Ochoa et al., 2007). We observed a similar summation phenomenon for NFATc3 in DRG neurons in response to trains of action potentials separated by 60 s (Fig. 2*B*). To further test the longevity of NFAT "memory," DRG neurons were stimulated by trains of action potentials (10 Hz for 10 s) spaced 15 min apart (Fig. 7*A*,*B*). Under control conditions, $[Ca^{2+}]_i$ responses showed the characteristic mitochondrion-dependent hump during the recovery phase. The nuclear level of NFATc3 rapidly increased after the first stimulus and remained elevated between the stimuli. In contrast, a combined treatment with antimycin and oligomycin eliminated the $[Ca^{2+}]_i$ hump and markedly suppressed the NFATc3 response, so that the nuclear/cytosolic ratio fully recovered before each subsequent stimulation (Fig. 7*B*). Thus, mitochondria contribute to the temporal summation of NFAT responses induced by repetitive neuronal activity.

To gain further insight into NFAT regulation in neurons, we plotted the extent of NFATc3 nuclear translocation as a function of the duration of the $[Ca^{2+}]_i$ response for all the data obtained using various protocols and treatments (Figs. 2, 4, 6). As shown in Figure 7*C*, this relationship was well described by the linear function (correlation coefficient $r^2 = 0.96$) across the broad range of stimulation protocols and pharmacological treatments, suggesting that the duration of NFAT residence in the nucleus is determined by the duration of $[Ca^{2+}]_i$ elevation. This also indicates that the mitochondrial inhibitors and the treatments targeting Ca^{2+} extrusion acted selectively at the level of Ca^{2+} signal generation, but that they did not directly affect downstream signaling steps such as nuclear import or export of NFAT.

Discussion

Ca^{2+} is the central regulator of excitation–transcription coupling in neurons (West et al., 2002; Fields et al., 2005). To date, most research has focused on the role of Ca^{2+} entry mechanisms in controlling specific transcription responses triggered by neuronal activity [for review, see Deisseroth et al. (2003) and Cohen and Greenberg (2008)]. We now present evidence that an additional level of transcriptional control is provided by systems that continue to shape Ca^{2+} signals even after Ca^{2+} entry is terminated. These systems include Ca^{2+} pumps and exchangers and Ca^{2+}-transporting organelles. Although all of these systems were known to significantly influence the spatial and temporal characteristics of neuronal Ca^{2+} signals (Miller, 1991; Thayer et al., 2002), their specific involvement in the control of neuronal gene expression remained largely unexplored.

Here we demonstrate for the first time that prolonged Ca^{2+} release from mitochondria facilitates activation of the tran-

scription factor NFAT in neurons. Moreover, we show that this effect additionally depends on Ca^{2+} extrusion via the plasma membrane Ca^{2+} pump and Na^+/Ca^{2+} exchanger. Based on our findings, we propose a model that incorporates mitochondrial Ca^{2+} cycling acting in concert with other Ca^{2+} transporters as a novel regulatory mechanism of excitation–transcription coupling in neurons (Fig. 7*D*). According to this model, the nuclear import of NFAT is triggered by Ca^{2+} influx via voltage- or ligand-gated Ca^{2+} channels. Ca^{2+} entering the cell is rapidly buffered by mitochondria and then is slowly released back to the cytosol via the mitochondrial Na^+/Ca^{2+} exchanger. The resulting prolonged $[Ca^{2+}]_i$ plateau, which is set by the balance between mitochondrial Ca^{2+} release and PMCA- and NCX-mediated Ca^{2+} extrusion, significantly extends NFAT residence within the nucleus, thereby facilitating NFAT transcriptional responses in neurons.

The critical role of NFAT in the nervous system is supported by a number of recent studies. NFAT is involved in the regulation of axonal growth, dendritic branching, and presynaptic differentiation (Yoshida and Mishina, 2005; Nguyen and Di Giovanni, 2008; Schwartz et al., 2009), and combined deletion of either NFATc3/NFATc4 or NFATc2/NFATc3/NFATc4 isoforms leads to a marked deficiency in axonal development (Graef et al., 2003). Moreover, NFATc2/NFATc4 double-knock-out mice show pronounced cognitive, behavioral, and neuromuscular defects that are reminiscent of the Down's syndrome phenotype (Arron et al., 2006). NFATc3 and NFATc4 have also been implicated in the regulation of neuronal survival (Benedito et al., 2005; Jayanthi et al., 2005; Luoma and Zirpel, 2008). Another likely function of NFAT is the long-term regulation of neuronal excitability. Indeed, NFAT regulates the expression of several K^+ channels, including voltage-gated $K_v1.5$, $K_v2.1$, $K_v4.2$, and $K_v4.3$ channels and the SK3 (small conductance Ca^{2+}-activated $K_{Ca}2.3$) channel (Sun et al., 2001; Amberg et al., 2004; Rossow et al., 2004), which are involved in the control of excitability and spike frequency adaptation in the central and peripheral neurons (Gutman et al., 2005). Notably, the expression of $K_v1.5$, $K_v2.1$, $K_v4.2$, and $K_v4.3$ appears to be controlled specifically by the NFATc3 isoform, at least in cardiac muscles (Rossow et al., 2004). In sensory neurons, NFAT mediates the expression of several pronociceptive genes, including COX-2, BDNF, and the chemokine receptor CCR2 (Groth et al., 2007; Jackson et al., 2007; Jung and Miller, 2008). COX-2 and BDNF have been linked to inflammatory pain (Svensson and Yaksh, 2002; McMahon et al., 2006), whereas CCR2 upregulation may contribute to the development of neuropathic pain (Jung and Miller, 2008). Therefore, the regulation of nociceptive plasticity is yet another function of NFAT.

Despite the importance of NFAT in the central and peripheral nervous systems, many questions remain about the mechanisms of NFAT regulation in neurons. By using simultaneous monitoring of $[Ca^{2+}]_i$ and NFAT translocation, we now provide new information on several important aspects of NFAT signaling in neurons. First, we found that an action potential-induced $[Ca^{2+}]_i$ increase triggers nuclear import of NFAT in sensory neurons with a relatively short delay of 30–40 s (Fig. 2*A*,*B*). This is consistent with the finding that >50% of NFAT becomes dephosphorylated within 1 min of stimulation with Ca^{2+} (Tomida et al., 2003). Second, we quantified NFAT activation as a function of $[Ca^{2+}]_i$ increase. We found that rather small $[Ca^{2+}]_i$ elevations (~200–300 nM) were sufficient to activate NFAT in DRG neurons. Importantly, several independent assays revealed similar $[Ca^{2+}]_i$ dependences. This includes examination of NFAT nuclear import in response to $[Ca^{2+}]_i$ elevations elicited by depolarization, cyclopiazonic acid, or ionomycin (Fig. 3*A–D*) (supplemental Figs. 3, 5, and 6, available at www.jneurosci.org as supplemental material), and the analysis of NFAT-luciferase expression mediated by endogenous NFATc proteins (Fig. 3*E*,*F*). The observed very steep, threshold-like $[Ca^{2+}]_i$ dependence of NFAT activation (Fig. 3*F*) is in good agreement with the highly cooperative Ca^{2+} dependence of CaN activation by calmodulin (Stemmer and Klee, 1994). Third, we found that induction of NFAT response depended on the activity of superoxide dismutase (Fig. 1*F*), an enzyme that protects CaN from superoxide radicals produced by mitochondria during a prolonged $[Ca^{2+}]_i$ elevation (Bito et al., 1996; Wang et al., 1996; Hongpaisan et al., 2003, 2004).

Most importantly, we found that prolonged Ca^{2+} release from mitochondria facilitates NFAT activation in sensory neurons. NFAT is exquisitely sensitive to the duration of the Ca^{2+} signal (Dolmetsch et al., 1997; Feske et al., 2001), which is imposed by the competition between CaN and NFAT kinases in controlling nuclear–cytosolic shuttling of NFAT. Ca^{2+}/CaN-dependent dephosphorylation of NFAT exposes the NLS and facilitates nuclear import of NFAT (Crabtree and Olson, 2002; Hogan et al., 2003). Upon termination of the $[Ca^{2+}]_i$ response, CaN dissociates from NFAT, allowing GSK3β and other NFAT kinases to rephosphorylate the transcription factor, thereby facilitating Crm-1-dependent nuclear export of NFAT (Beals et al., 1997; Chow et al., 1997; Okamura et al., 2000). Thus, a prolonged $[Ca^{2+}]_i$ elevation is required to sustain CaN activation and to induce the NFAT-mediated transcriptional response.

In immune and other nonexcitable cells, prolonged $[Ca^{2+}]_i$ elevation is enabled by a capacitative Ca^{2+} influx via CRAC channels (Feske et al., 2006; Putney, 2007). Our work now demonstrates that in neurons, a similar role in the NFAT activation process can be attributed to the mitochondrion. By steadily releasing Ca^{2+} accumulated during neuronal stimulation, this organelle markedly extends the elevation in $[Ca^{2+}]_i$ beyond the short duration of an action potential train or TRPV1 activation, and the $[Ca^{2+}]_i$ levels during the mitochondrion-dependent plateau phase are well within the range of those required for NFAT activation. Interestingly, in T-lymphocytes mitochondria can also contribute to the regulation of NFAT, although through a different mechanism (Hoth et al., 2000; Chen et al., 2007). Whereas NFAT activation in sensory neurons is facilitated directly by the release of Ca^{2+} from mitochondria (Figs. 4, 5), in T-lymphocytes, the underlying mechanism seems to be Ca^{2+} buffering by mitochondria and, consequently, a prevention of Ca^{2+}-dependent inactivation of CRAC channels (Hoth et al., 2000). In addition, it was reported that genetic disruption of the mitochondrial respiratory chain prevents NFAT-dependent heart formation in *Xenopus laevis* and inhibits NFAT signaling in HeLa and Jurkat cells, most likely as a result of ATP depletion (Chen et al., 2007). It is unlikely that the ATP depletion contributed appreciably to our findings, however. First, in our work the electron transport inhibitor antimycin was always applied in the presence of the ATP synthase inhibitor oligomycin. Such combined treatment produces mitochondrial depolarization without a loss of ATP, as ATP can be maintained in cultured neurons via glycolysis (Nicholls and Budd, 2000) (also see supplemental Fig. 7, available at www.jneurosci.org as supplemental material). Second, we found that an inhibitor of mitochondrial Na^+/Ca^{2+} exchange, CGP37157, which is known to increase cellular ATP production (Visch et al., 2004), also eliminated the Ca^{2+} plateau

and inhibited NFAT activation in DRG neurons, similarly to the effects of antimycin/oligomycin treatment.

Our mtPericam $[Ca^{2+}]_{mt}$ measurements indicated that mitochondria throughout the cell body were engaged in Ca^{2+} storage and release, including mitochondria adjacent to the nucleus (Fig. 2*E*,*F*). Ca^{2+} released from perinuclear mitochondria was the likely source of the prolonged $[Ca^{2+}]_i$ elevation within the nucleus, which could be important for maintaining the CaN–NFAT interaction and thus for preventing Crm-1-mediated nuclear export of NFAT (Zhu and McKeon, 1999). Pharmacological disruption of mitochondrial Ca^{2+} transport eliminated the $[Ca^{2+}]_i$ plateau in both the cytosol and the nucleus and significantly diminished NFAT nuclear import and NFAT-mediated transcription. Furthermore, mitochondrial inhibitors prevented the temporal summation of nuclear NFAT responses induced by repetitive bursts of action potentials (Fig. 7).

Taken together, our data suggest that Ca^{2+} cycling by mitochondria promotes NFAT activation in neurons and facilitates the function of NFAT as a nuclear integrator of repetitive electrical activity. Given the ability of mitochondria to markedly reduce the magnitude and prolong the duration of Ca^{2+} signals, and to affect propagation of Ca^{2+} elevation to the nucleus (Park et al., 2001), it is likely that the mechanism described here is of general importance for neuronal gene regulation and that many other Ca^{2+}-dependent transcription factors (e.g., CREB, CaRF, and MEF2) will also be differentially modulated by mitochondria. The net result will ultimately be defined by the sensitivity of a specific transcription factor to the amplitude and duration of Ca^{2+} signals and by its proximity to mitochondria and other competing Ca^{2+} buffers.

References

Amberg GC, Rossow CF, Navedo MF, Santana LF (2004) NFATc3 regulates Kv2.1 expression in arterial smooth muscle. J Biol Chem 279:47326–47334.

Aramburu J, Yaffe MB, López-Rodríguez C, Cantley LC, Hogan PG, Rao A (1999) Affinity-driven peptide selection of an NFAT inhibitor more selective than cyclosporin A. Science 285:2129–2133.

Arron JR, Winslow MM, Polleri A, Chang CP, Wu H, Gao X, Neilson JR, Chen L, Heit JJ, Kim SK, Yamasaki N, Miyakawa T, Francke U, Graef IA, Crabtree GR (2006) NFAT dysregulation by increased dosage of DSCR1 and DYRK1A on chromosome 21. Nature 441:595–600.

Baron KT, Thayer SA (1997) CGP37157 modulates mitochondrial Ca^{2+} homeostasis in cultured rat dorsal root ganglion neurons. Eur J Pharmacol 340:295–300.

Beals CR, Sheridan CM, Turck CW, Gardner P, Crabtree GR (1997) Nuclear export of NF-ATc enhanced by glycogen synthase kinase-3. Science 275:1930–1934.

Benedito AB, Lehtinen M, Massol R, Lopes UG, Kirchhausen T, Rao A, Bonni A (2005) The transcription factor NFAT3 mediates neuronal survival. J Biol Chem 280:2818–2825.

Bhave G, Gereau RW 4th (2004) Posttranslational mechanisms of peripheral sensitization. J Neurobiol 61:88–106.

Bito H, Deisseroth K, Tsien RW (1996) CREB phosphorylation and dephosphorylation - a Ca2(+)- and stimulus duration-dependent switch for hippocampal gene expression. Cell 87:1203–1214.

Brosenitsch TA, Katz DM (2001) Physiological patterns of electrical stimulation can induce neuronal gene expression by activating N-type calcium channels. J Neurosci 21:2571–2579.

Budd SL, Nicholls DG (1996) A reevaluation of the role of mitochondria in neuronal Ca2+ homeostasis. J Neurochem 66:403–411.

Camello C, Lomax R, Petersen OH, Tepikin AV (2002) Calcium leak from intracellular stores—the enigma of calcium signalling. Cell Calcium 32:355–361.

Caterina MJ, Julius D (2001) The vanilloid receptor: a molecular gateway to the pain pathway. Annu Rev Neurosci 24:487–517.

Chen Y, Yuen WH, Fu J, Huang G, Melendez AJ, Ibrahim FB, Lu H, Cao X (2007) The mitochondrial respiratory chain controls intracellular calcium signaling and NFAT activity essential for heart formation in *Xenopus laevis*. Mol Cell Biol 27:6420–6432.

Chin ER, Olson EN, Richardson JA, Yang Q, Humphries C, Shelton JM, Wu H, Zhu W, Bassel-Duby R, Williams RS (1998) A calcineurin-dependent transcriptional pathway controls skeletal muscle fiber type. Genes Dev 12:2499–2509.

Chow CW, Rincón M, Cavanagh J, Dickens M, Davis RJ (1997) Nuclear accumulation of NFAT4 opposed by the JNK signal transduction pathway. Science 278:1638–1641.

Cohen S, Greenberg ME (2008) Communication between the synapse and the nucleus in neuronal development, plasticity, and disease. Annu Rev Cell Dev Biol 24:183–209.

Colegrove SL, Albrecht MA, Friel DD (2000) Dissection of mitochondrial Ca^{2+} uptake and release fluxes in situ after depolarization-evoked $[Ca^{2+}]_i$ elevations in sympathetic neurons. J Gen Physiol 115:351–370.

Crabtree GR, Olson EN (2002) NFAT signaling: choreographing the social lives of cells. Cell 109 [Suppl]:S67–S79.

David G (1999) Mitochondrial clearance of cytosolic Ca^{2+} in stimulated lizard motor nerve terminals proceeds without progressive elevation of mitochondrial matrix $[Ca^{2+}]$. J Neurosci 19:7495–7506.

Deisseroth K, Mermelstein PG, Xia H, Tsien RW (2003) Signaling from synapse to nucleus: the logic behind the mechanisms. Curr Opin Neurobiol 13:354–365.

Dolmetsch RE, Lewis RS, Goodnow CC, Healy JI (1997) Differential activation of transcription factors induced by Ca2+ response amplitude and duration. Nature 386:855–858.

Eshete F, Fields RD (2001) Spike frequency decoding and autonomous activation of Ca^{2+}-calmodulin-dependent protein kinase II in dorsal root ganglion neurons. J Neurosci 21:6694–6705.

Feske S, Giltnane J, Dolmetsch R, Staudt LM, Rao A (2001) Gene regulation mediated by calcium signals in T lymphocytes. Nat Immunol 2:316–324.

Feske S, Gwack Y, Prakriya M, Srikanth S, Puppel SH, Tanasa B, Hogan PG, Lewis RS, Daly M, Rao A (2006) A mutation in Orai1 causes immune deficiency by abrogating CRAC channel function. Nature 441:179–185.

Fields RD, Eshete F, Stevens B, Itoh K (1997) Action potential-dependent regulation of gene expression: temporal specificity in Ca^{2+}, cAMP-responsive element binding proteins, and mitogen-activated protein kinase signaling. J Neurosci 17:7252–7266.

Fields RD, Lee PR, Cohen JE (2005) Temporal integration of intracellular Ca2+ signaling networks in regulating gene expression by action potentials. Cell Calcium 37:433–442.

Friel DD (2000) Mitochondria as regulators of stimulus-evoked calcium signals in neurons. Cell Calcium 28:307–316.

García-Chacón LE, Nguyen KT, David G, Barrett EF (2006) Extrusion of Ca2+ from mouse motor terminal mitochondria via a Na+-Ca2+ exchanger increases post-tetanic evoked release. J Physiol 574:663–675.

Graef IA, Mermelstein PG, Stankunas K, Neilson JR, Deisseroth K, Tsien RW, Crabtree GR (1999) L-type calcium channels and GSK-3 regulate the activity of NF-ATc4 in hippocampal neurons. Nature 401:703–708.

Graef IA, Wang F, Charron F, Chen L, Neilson J, Tessier-Lavigne M, Crabtree GR (2003) Neurotrophins and netrins require calcineurin/NFAT signaling to stimulate outgrowth of embryonic axons. Cell 113:657–670.

Greer PL, Greenberg ME (2008) From synapse to nucleus: calcium-dependent gene transcription in the control of synapse development and function. Neuron 59:846–860.

Groth RD, Mermelstein PG (2003) Brain-derived neurotrophic factor activation of NFAT (nuclear factor of activated T-cells)-dependent transcription: a role for the transcription factor NFATc4 in neurotrophin-mediated gene expression. J Neurosci 23:8125–8134.

Groth RD, Coicou LG, Mermelstein PG, Seybold VS (2007) Neurotrophin activation of NFAT-dependent transcription contributes to the regulation of pro-nociceptive genes. J Neurochem 102:1162–1174.

Grynkiewicz G, Poenie M, Tsien RY (1985) A new generation of Ca^{2+} indicators with greatly improved fluorescence properties. J Biol Chem 260:3440–3450.

Gutman GA, Chandy KG, Grissmer S, Lazdunski M, McKinnon D, Pardo LA, Robertson GA, Rudy B, Sanguinetti MC, Stühmer W, Wang X (2005) International Union of Pharmacology. LIII. Nomenclature and molecular relationships of voltage-gated potassium channels. Pharmacol Rev 57:473–508.

Hernández-Ochoa EO, Contreras M, Cseresnyés Z, Schneider MF (2007) Ca2+ signal summation and NFATc1 nuclear translocation in sympa-

thetic ganglion neurons during repetitive action potentials. Cell Calcium 41:559–571.
Herrington J, Park YB, Babcock DF, Hille B (1996) Dominant role of mitochondria in clearance of large Ca^{2+} loads from rat adrenal chromaffin cells. Neuron 16:219–228.
Hogan PG, Chen L, Nardone J, Rao A (2003) Transcriptional regulation by calcium, calcineurin, and NFAT. Genes Dev 17:2205–2232.
Hongpaisan J, Winters CA, Andrews SB (2003) Calcium-dependent mitochondrial superoxide modulates nuclear CREB phosphorylation in hippocampal neurons. Mol Cell Neurosci 24:1103–1115.
Hongpaisan J, Winters CA, Andrews SB (2004) Strong calcium entry activates mitochondrial superoxide generation, upregulating kinase signaling in hippocampal neurons. J Neurosci 24:10878–10887.
Hoth M, Button DC, Lewis RS (2000) Mitochondrial control of calcium-channel gating: a mechanism for sustained signaling and transcriptional activation in T lymphocytes. Proc Natl Acad Sci U S A 97:10607–10612.
Huang SM, Bisogno T, Trevisani M, Al-Hayani A, De Petrocellis L, Fezza F, Tognetto M, Petros TJ, Krey JF, Chu CJ, Miller JD, Davies SN, Geppetti P, Walker JM, Di Marzo V (2002) An endogenous capsaicin-like substance with high potency at recombinant and native vanilloid VR1 receptors. Proc Natl Acad Sci U S A 99:8400–8405.
Jackson JG, Usachev YM, Thayer SA (2007) Bradykinin-induced NFAT-dependent transcription in rat dorsal root ganglion neurons. Mol Pharmacol 72:303–310.
Jayanthi S, Deng X, Ladenheim B, McCoy MT, Cluster A, Cai NS, Cadet JL (2005) Calcineurin/NFAT-induced up-regulation of the Fas ligand/Fas death pathway is involved in methamphetamine-induced neuronal apoptosis. Proc Natl Acad Sci U S A 102:868–873.
Jung H, Miller RJ (2008) Activation of the nuclear factor of activated T-cells (NFAT) mediates upregulation of CCR2 chemokine receptors in dorsal root ganglion (DRG) neurons: a possible mechanism for activity-dependent transcription in DRG neurons in association with neuropathic pain. Mol Cell Neurosci 37:170–177.
Lu SG, Zhang X, Gold MS (2006) Intracellular calcium regulation among subpopulations of rat dorsal root ganglion neurons. J Physiol 577:169–190.
Luoma JI, Zirpel L (2008) Deafferentation-induced activation of NFAT (nuclear factor of activated T-cells) in cochlear nucleus neurons during a developmental critical period: a role for NFATc4-dependent apoptosis in the CNS. J Neurosci 28:3159–3169.
McMahon SB, Bennett DL, Bevan S (2006) Inflammatory mediators and modulators of pain. In: Textbook of pain (McMahon SB, Koltzenburg M, eds), pp 49–72. London: Elsevier.
Medvedeva YV, Kim MS, Usachev YM (2008) Mechanisms of prolonged presynaptic Ca^{2+} signaling and glutamate release induced by TRPV1 activation in rat sensory neurons. J Neurosci 28:5295–5311.
Meyer RA, Campbell JN (1981) Myelinated nociceptive afferents account for the hyperalgesia that follows a burn to the hand. Science 213:1527–1529.
Miller RJ (1991) The control of neuronal Ca^{2+} homeostasis. Prog Neurobiol 37:255–285.
Nagai T, Sawano A, Park ES, Miyawaki A (2001) Circularly permuted green fluorescent proteins engineered to sense Ca2+. Proc Natl Acad Sci U S A 98:3197–3202.
Nguyen T, Di Giovanni S (2008) NFAT signaling in neural development and axon growth. Int J Dev Neurosci 26:141–145.
Nicholls DG, Budd SL (2000) Mitochondria and neuronal survival. Physiol Rev 80:315–360.
Nieves-Cintrón M, Amberg GC, Navedo MF, Molkentin JD, Santana LF (2008) The control of Ca2+ influx and NFATc3 signaling in arterial smooth muscle during hypertension. Proc Natl Acad Sci U S A 105:15623–15628.
Okamura H, Aramburu J, García-Rodríguez C, Viola JP, Raghavan A, Tahiliani M, Zhang X, Qin J, Hogan PG, Rao A (2000) Concerted dephosphorylation of the transcription factor NFAT1 induces a conformational switch that regulates transcriptional activity. Mol Cell 6:539–550.
Oliveria SF, Dell'Acqua ML, Sather WA (2007) AKAP79/150 anchoring of calcineurin controls neuronal L-type Ca2+ channel activity and nuclear signaling. Neuron 55:261–275.
Park MK, Ashby MC, Erdemli G, Petersen OH, Tepikin AV (2001) Perinuclear, perigranular and sub-plasmalemmal mitochondria have distinct functions in the regulation of cellular calcium transport. EMBO J 20:1863–1874.
Pivovarova NB, Hongpaisan J, Andrews SB, Friel DD (1999) Depolarization-induced mitochondrial Ca accumulation in sympathetic neurons: spatial and temporal characteristics. J Neurosci 19:6372–6384.
Putney JW Jr (2007) Recent breakthroughs in the molecular mechanism of capacitative calcium entry (with thoughts on how we got here). Cell Calcium 42:103–110.
Rossow CF, Minami E, Chase EG, Murry CE, Santana LF (2004) NFATc3-induced reductions in voltage-gated K+ currents after myocardial infarction. Circ Res 94:1340–1350.
Schnizler K, Shutov LP, Van Kanegan MJ, Merrill MA, Nichols B, McKnight GS, Strack S, Hell JW, Usachev YM (2008) Protein kinase A anchoring via AKAP150 is essential for TRPV1 modulation by forskolin and prostaglandin E2 in mouse sensory neurons. J Neurosci 28:4904–4917.
Schwartz N, Schohl A, Ruthazer ES (2009) Neural activity regulates synaptic properties and dendritic structure in vivo through calcineurin/NFAT signaling. Neuron 62:655–669.
Schwiening CJ, Kennedy HJ, Thomas RC (1993) Calcium hydrogen exchange by the plasma membrane Ca-ATPase of voltage-clamped snail neurons. Proc R Soc Lond 253:285–289.
Slugg RM, Meyer RA, Campbell JN (2000) Response of cutaneous A- and C-fiber nociceptors in the monkey to controlled-force stimuli. J Neurophysiol 83:2179–2191.
Stemmer PM, Klee CB (1994) Dual calcium ion regulation of calcineurin by calmodulin and calcineurin B. Biochemistry 33:6859–6866.
Sun G, Tomita H, Shakkottai VG, Gargus JJ (2001) Genomic organization and promoter analysis of human KCNN3 gene. J Hum Genet 46:463–470.
Svensson CI, Yaksh TL (2002) The spinal phospholipase-cyclooxygenase-prostanoid cascade in nociceptive processing. Annu Rev Pharmacol Toxicol 42:553–583.
Szallasi A, Cortright DN, Blum CA, Eid SR (2007) The vanilloid receptor TRPV1: 10 years from channel cloning to antagonist proof-of-concept. Nat Rev Drug Discov 6:357–372.
Thayer SA, Usachev YM, Pottorf WJ (2002) Modulating Ca^{2+} clearance from neurons. Front Biosci 7:d1255–d1279.
Tomida T, Hirose K, Takizawa A, Shibasaki F, Iino M (2003) NFAT functions as a working memory of Ca2+ signals in decoding Ca2+ oscillation. EMBO J 22:3825–3832.
Usachev Y, Shmigol A, Pronchuk N, Kostyuk P, Verkhratsky A (1993) Caffeine-induced calcium release from internal stores in cultured rat sensory neurons. Neuroscience 57:845–859.
Usachev YM, Thayer SA (1999) Ca^{2+} influx in resting rat sensory neurones that regulates and is regulated by ryanodine-sensitive Ca^{2+} stores. J Physiol 519:115–130.
Usachev YM, DeMarco SJ, Campbell C, Strehler EE, Thayer SA (2002) Bradykinin and ATP accelerate Ca^{2+} efflux from rat sensory neurons via protein kinase C and the plasma membrane Ca^{2+} pump isoform 4. Neuron 33:113–122.
Usachev YM, Marsh AJ, Johanns TM, Lemke MM, Thayer SA (2006) Activation of protein kinase C in sensory neurons accelerates Ca^{2+} uptake into the endoplasmic reticulum. J Neurosci 26:311–318.
Visch HJ, Rutter GA, Koopman WJ, Koenderink JB, Verkaart S, de Groot T, Varadi A, Mitchell KJ, van den Heuvel LP, Smeitink JA, Willems PH (2004) Inhibition of mitochondrial Na+-Ca2+ exchange restores agonist-induced ATP production and Ca2+ handling in human complex I deficiency. J Biol Chem 279:40328–40336.
Wang X, Culotta VC, Klee CB (1996) Superoxide dismutase protects calcineurin from inactivation. Nature 383:434–437.
West AE, Griffith EC, Greenberg ME (2002) Regulation of transcription factors by neuronal activity. Nat Rev Neurosci 3:921–931.
Yoshida T, Mishina M (2005) Distinct roles of calcineurin-nuclear factor of activated T-cells and protein kinase A–cAMP response element-binding protein signaling in presynaptic differentiation. J Neurosci 25:3067–3079.
Zhu J, McKeon F (1999) NF-AT activation requires suppression of Crm1-dependent export by calcineurin. Nature 398:256–260.